The Thesis Committee for Marlo Rose Gawey
Certifies that this is the approved version of the following thesis:

Experimental Analysis and Modeling of Perfluorocarbon Transport in the Vadose Zone: Implications for Monitoring CO_2 Leakage at CCS Sites

APPROVED BY
SUPERVISING COMMITTEE:

Supervisor:

Daniel O. Breecker

Katherine D. Romanak, Co-Supervisor

Toti E. Larson, Co-Supervisor

Michael H. Young

Experimental Analysis and Modeling of Perfluorocarbon Transport in the Vadose Zone: Implications for Monitoring CO_2 Leakage at CCS Sites

by

Marlo Rose Gawey, B.S.

Thesis

Presented to the Faculty of the Graduate School of

The University of Texas at Austin

in Partial Fulfillment

of the Requirements

for the Degree of

Master of Science in Geological Sciences

The University of Texas at Austin

May 2013

Acknowledgements

I would like to thank my committee, Dan, Katherine, Toti and Michael for their support throughout this project. I am very fortunate to have been advised by such excellent people and I am a better scientist due to their guidance. I'd particularly like to thank Toti for squeezing this project into his busy schedule, being endlessly patient, and clueing me in to lots of great new music. Thank you to Sue Hovorka who has overseen this project and offered lots of helpful advice and research opportunities. This project was funded by the Gulf Coast Carbon Center at the Bureau of Economic Geology.

Soil samples were generously provided by Veronica Anderson and Lia Bresson. Additional analyses were performed by Tongwei Zhang and Xun Sun (BET analyses), Todd Caldwell (particle size distribution), and Miguel Cisneros (XRD). Tommy Joe Phelps and Susan Pfiffner taught me the ins-and-outs of PFT analysis and graciously hosted Theodore and me during our summer at Oak Ridge National Laboratory.

None of this would have been possible without my friends and family. My fellow students at the "G triple C" have provided many helpful discussions and many more helpful distractions. My siblings, John and Colleen, are my best friends, staunchest allies, and fiercest critics. They've been cheering me on since I decided to study rocks six years ago and I couldn't ask for better. And finally, to my parents, Steve and Jan Gawey: thank you for… well, where do I begin? All of my accomplishments are due entirely to your love and support. I love you very, very much. You're the best.

Abstract

Experimental Analysis and Modeling of Perfluorocarbon Transport in the Vadose Zone: Implications for Monitoring CO_2 Leakage at CCS Sites

Marlo Rose Gawey, M.S. Geo. Sci.

The University of Texas at Austin, 2013

Supervisors: Daniel Breecker, Katherine Romanak, Toti Larson

Perfluorocarbon tracers (PFTs) are commonly proposed tracers for use in carbon capture and sequestration (CCS) leak detection and vadose zone monitoring programs. Tracers are co-injected with supercritical CO_2 and monitored in the vadose zone to identify leakage and calculate leakage rates. These calculations assume PFTs exhibit "ideal" tracer behavior (i.e. do not sorb onto or react with porous media, partition into liquid phases or undergo decay). This assumption has been brought into question by lab and field evaluations showing PFT partitioning into soil contaminants and sorbing onto clay. The objective of this study is to identify substrates in which PFTs behave conservatively and quantify non-conservative behavior. PFT breakthrough curves are compared to those of a second, conservative tracer, sulfur hexafluoride (SF_6). Breakthrough curves are generated in 1D flow-through columns packed with 5 different substrates: silica beads, quartz sand, illite, organic-rich soil, and organic-poor soil.

Constant flow rate of carrier gas, N_2, is maintained. A known mass of tracer is injected at the head of the columns and the effluent analyzed at regular intervals for tracers at picogram levels by gas chromatography. PFT is expected to behave conservatively with respect to SF_6 in silica beads or quartz sand and non-conservatively in columns with clay or organics. However, results demonstrate PFT retardation with respect to SF_6 in all media (retardation factor is 1.1 in silica beads and quartz sand, 2.5 in organic-rich soil, >20 in organic-poor soil, and >100 in illite). Retardation is most likely due to sorption onto clays and soil organic matter or condensation to the liquid phase. Sorption onto clays appears to be the most significant factor. Experimental data are consistent with an analytical advection/diffusion model. These results show that PFT retardation in the vadose zone has not been adequately considered for interpretation of PFT data for CCS monitoring. These results are preliminary and do not take into account more realistic vadose zone conditions such as the presence of water, in which PFTs are insoluble. Increased moisture content will likely decrease sorption onto porous media and retardation in the vadose zone may be less than determined in these experiments.

Table of Contents

List of Tables

List of Figures

1. Introduction

1.1 CARBON CAPTURE AND STORAGE

The current increase in atmospheric CO_2 concentrations is determined to be dominantly caused by anthropogenic emissions from fossil fuel burning and land use change (IPCC, 2007). Climate change due to the increase in atmospheric CO_2 has resulted in a decrease in ocean pH (Caldeira and Wickett, 2003; Orr et al., 2005; Doney et al., 2009) and an increase in ice sheet melting (Thomas et al., 2004; Joughin et al., 2012; Shepherd et al., 2012), among other global changes, and will continue to contribute to atmospheric warming and sea level rise (IPCC, 2007; Spada et al., 2013). No single approach is sufficient to mitigate CO_2 emissions; the portfolio of necessary actions will include increasing energy efficiency, increasing use of renewable energies and nuclear power, and using advanced technologies to reduce CO_2 emissions to the atmosphere (IEA, 2009).

To meet goals for climate change mitigation—such as those called for by the United Nations Framework Convention on Climate Change, of which The United States is a signatory—carbon capture and sequestration (CCS) will be a crucial technology. CCS involves the separation and capture of CO_2 emissions from point sources, such as coal fired power plants, compression of CO_2 to a supercritical fluid, and injection into a geologic storage location for permanent storage. The U.S. Department of Energy projects coal fired power plants to continue to make up 43% of U.S. energy generation through 2035 (EIA, 2011). The International Energy Agency concluded that CCS could provide 19% of the reduction in CO_2 emissions required to stabilize CO_2 concentration at

450 parts per million by 2050, even while energy demand continues to grow (IEA, 2009). CCS allows for continued production of cost-effective fossil fuel-based electricity while renewable and nuclear energy production matures. For this reason, it is sometimes called a "bridging" technology to facilitate the transition (Watson and Sullivan, 2012). By one estimate, implementation of CCS can reduce costs of emissions mitigation by 70% (IEA, 2009).

CCS is designed to reduce emissions from large stationary sources of CO_2. The North American Carbon Storage Atlas identifies 4,245 such sources in North America alone, amounting to 3,729 million metric tons of CO_2 emitted per year (NETL, 2012). These sources include iron and steel mills, petroleum refineries, various chemical plants, and coal fired power plants. The latter makes up about one third of U.S. CO_2 emissions and supplies 50% of U.S. energy generation, making coal fired power plants a particularly important target for CCS development (MIT, 2007; IEA, 2009). CCS technologies can reduce CO_2 emissions from a coal fired power plant by 80%-90%, a significant contribution to mitigation efforts (IPCC, 2005; MIT, 2007).

1.2 MONITORING AND VERIFICATION

Testing and monitoring for fluid migration out of the injection area are expected to be a requirement of future geologic storage projects (USEPA, 2010). CO_2 will tend to rise and potentially find leakage pathways out of the reservoir (IPCC, 2005). Testing and monitoring refers to the collection of activities designed to detect fluid migration or risk factors for fluid migration which could endanger underground sources of drinking water (USDWs) or release CO_2 into the atmosphere (USEPA, 2010). The goals of monitoring

are to provide data to confirm the integrity of the cap rock, to provide confidence that public health and safety are ensured, and to provide an early warning system to effectively mitigate any unforeseen leakage (Schütze et al., 2012). Optimum designs will likely be site-specific, multi-disciplinary monitoring plans which use a variety of techniques at different depths including collection and analysis of groundwater and soil gas, pressure measurement, and geophysical techniques (DOE/NETL, 2012).

Monitoring and verification activities can take place at any location within or above the injection zone. However, observations in the near-surface monitoring zone (NSMZ), illustrated in Figure 1-1, are of particular interest for monitoring and verification schemes because they apply directly to areas of special interest for regulators and public health and safety: aquifers, the vadose zone, and the atmosphere.

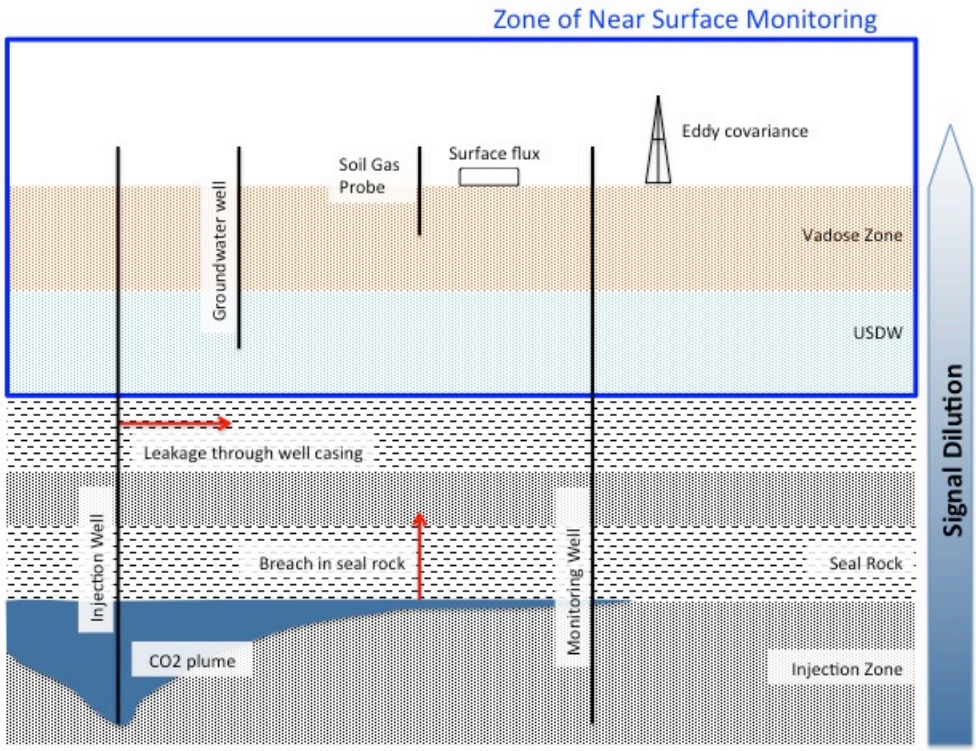

Figure 1-1: Diagram of near-surface monitoring locations and techniques above a CCS injection zone with two leakage scenarios.

However, direct monitoring techniques for CO_2 in the NSMZ such as soil gas collection and surface flux measurements are met with two key problems: dilution of CO_2 from the injection zone to the surface and the variability of CO_2 concentration and flux in both time and space. This signal-to-background issue makes leakage detection difficult, particularly in the case of small rates of seepage over broad areas.

1.3 TRACERS: GENERAL INTRODUCTION

Tracers offer a unique solution to the signal-to-background challenge. Tracers are chemical compounds chosen for their low detection limits and very low background

levels that do not vary widely, thus increasing the signal-to-background ratio for leakage detection. Tracers are co-injected with sequestered CO_2 and then sampled in lieu of, or in addition to, direct testing for CO_2. The presence of tracers in the NSMZ is evidence for a leakage pathway from the injection zone to the NSMZ and the possibility for CO_2 leakage.

Common tracers for CCS projects include isotopically labeled gases, noble gases, and synthetic chemicals like SF_6 and perfluorocarbon tracers (PFTs). One or several of these tracers can be used in a single CCS project to give the injected CO_2 a unique "fingerprint" both within the reservoir and in the NSMZ. Tracer concentrations in the NSMZ are used to evaluate the presence of leakage from the injection zone as well as to quantify the potential rate of leakage from the reservoir to the NSMZ.

PFTs, in particular, have been singled out for use in several large-scale CCS demonstration projects for monitoring in the NSMZ (McCallum et al., 2005). For these projects, PFTs are assumed conservative (i.e. nonreactive, non-sorbing, non-partitioning) and PFT concentrations in the NSMZ are used to test for and quantify leakage rates. If PFTs are reacted with, sorbed onto, or partitioned into the geologic media in the NSMZ, leakage rates based on PFTs will be inaccurate or leakage will not be detected.

The assumption that PFTs are conservative has not been substantiated lab and field evaluations. Lab and field evaluations have shown that PFTs are reactive with some common contaminants in the vadose zone, such as light non-aqueous phase liquids

(LNAPL). Starting in the mid-1990s, PFTs have been successfully used as partitioning tracers to quantify the volume of LNAPL in contamination soils (Jin et al., 1995; Whitley et al., 1999; Deeds et al., 2000). This is due to PFT solubility in LNAPLs. Additionally, retention of two perfluorocarbons (PMCP and PMCH) was shown to be increased up to 10% in the presence of kaolinite and up to 20% in the presence of liquid decane (Dugstad et al., 1993). Moisture content in packed sand columns has also been shown to have a strong effect on tracer retention times of five PFTs (PDCP, PMCP, PMCH, o-PDCH and PTCH). PFTs showed longer retention times and retardation in dry sand columns and showed conservative behavior in dampened sand columns (Maxfield et al., 2005).

SF_6 is another tracer chosen for CCS demonstration projects, though less commonly than PFT. In contrast to PFT, SF_6, is shown to be an ideal tracer in many different substrates (Olschewski et al., 1995; Wilson and Mackay, 1996; Gamlin et al., 2001; Santella et al., 2003). SF_6 has a long history as an environmental tracer in groundwater (e.g. Busenberg and Plummer, 2000) and the vadose zone (e.g. Tick et al., 2007). It has been used as a conservative tracer for the purpose of comparisons with non-conservative tracers in one dimensional column experiments (Mariner et al., 1999) and field tests (Keller and Brusseau, 2003).

Given this evidence, SF_6 might be considered a preferable tracer for CCS monitoring and verification. However, SF_6 has higher background concentrations than that of PFT due to its long history as an environmental tracer. Also, because SF_6 has a

high global warming potential and is widely used in the electric power industry, SF_6 is subject to stricter regulations than are PFTs. In the European Union, SF_6 emissions have been regulated since 2006 (Regulation(EC) No 842/2006). Since 1999, the U.S. EPA has maintained a voluntary SF_6 emission reduction program called the "SF_6 Emission Reduction Partnership for Electric Power Systems" and in 2008 SF_6 was added to the U.S. Department of Defense Emerging Contaminants Action Program" (USEPA, 2011; USDOD, 2012). SF_6 is also regulated under the Kyoto Protocol (Rigby et al., 2010). For these reason, SF_6 may not be the best long-term option as a CCS tracer.

1.4 OBJECTIVES AND HYPOTHESIS

The objectives of this project are to 1) identify under what conditions PFTs behave conservatively with respect to SF_6, 2) to quantify the retardation factors for conditions that produce non-conservative behavior, and 3) develop an analytical model that can adequately describe these transport phenomena and be used to interpret tracer breakthrough curves.

This will be accomplished by comparing tracer breakthrough curves for PFT and SF_6 in one-dimensional flow through columns packed with materials of interest and fitting experimental data for SF_6 breakthrough curves with an analytical model. For the purposes of this study, SF_6 will be assumed conservative. The delay in PFT residence time with respect to the SF_6 residence time will determine the degree to which PFT does or does not behave conservatively.

I hypothesize that PFT will not have delayed transport compared to SF_6 in columns packed with silica beads or quartz sand (i.e. PFT will behave conservatively) and PFT will have delayed transport compared to SF_6 in columns with added organic carbon or clay (i.e. PFT will behave non-conservatively).

2. Background

In this section, I will discuss 1) the challenges of monitoring in the NSMZ and how tracers can uniquely meet these challenges, 2) the historical use of PFT and SF_6 relevant to CCS applications, and 3) a general chemical background of SF_6 and PFTs.

2.1 NSMZ

The NSMZ includes the aquifers, vadose zone and atmosphere overlying a CCS project and does not include the zone directly overlying the injection zone, also known as the above-zone monitoring interval (AZMI). Near-surface monitoring schemes generally aim to detect leakage by direct measurement of CO_2 concentration or flux to the aquifer, vadose zone, or atmosphere (Klusman, 2011). Technologies to accomplish this goal include direct sampling and analysis of vadose zone and atmospheric gases, sampling and geochemical analyses of aquifer fluid, eddy covariance, and LIDAR (Klusman, 2011; Watson and Sullivan, 2012).

There are several challenges facing direct measurement of CO_2 concentration and flux in NSMZ. The background concentration and flux of CO_2 in the vadose zone varies widely in both time and space (Lewicki, 2005; Cannavo et al., 2006; Cortis et al., 2008). This variation is due to both natural (e.g. diurnal cycling, seasonal variations) and anthropogenic (e.g. the presence of CO_2 emitting power plants) effects (Luo and Zhou, 2006). Additionally, leaked CO_2 is likely to be diluted or reacted along the pathway from reservoir to surface, such that the CO_2 signal becomes difficult to detect in the vadose

zone and atmosphere. This is particularly the case for low rates of seepage, often called "microseepage" (Klusman, 2011). Due to the high variability of naturally occurring CO_2 and dilution of leaked gas, the signal-to-background ratio for leakage detection at the surface is very low. Therefore, many plans have recommended 1 year or more of background CO_2 concentration measurements at each prospective CCS site to characterize the background variability (DOE/NETL, 2012; USEPA, 2013; Schloemer et al., 2013).

In contrast, tracers are designed to have low background concentration as well as very low detection limits. Tracers are often manufactured and have no natural sources. Thus, the signal-to-background ratio for these tracers is increased, as are the likelihood of finding a leakage and the sensitivity of the monitoring program to microseepage. The presence of tracers in the vadose zone is evidence for a leakage pathway for gases from the injection zone to the NSMZ and is not necessarily evidence for the presence of gaseous injected CO_2 in the vadose zone. CO_2 is reactive and may become dissolved in fluids, precipitated into solid phase, or react with other constituents in the subsurface.

Tracers can also yield important information in the injection zone. Tracer concentrations measured at monitoring wells can be used to monitor CO_2 arrival as well as unequivocally verify the presence of injected CO_2 at monitoring wells (Stalker et al., 2009). For example, in 2004, slugs of tracers were co-injected with ~1600 tonnes of supercritical CO2 into the Frio brine aquifer and were used for quantification of plume

breakthrough and transport time and better understanding of preferential flow paths (McCallum et al., 2005).

2.2 HISTORY OF PFTS AND SF_6 AS CCS TRACERS

Several desirable characteristics are widely agreed upon for CCS tracers (Senum et al., 1992; Maxfield et al., 2005; Watson et al., 2007; Reimus et al., 2011). The tracer must be:

(1) stable

(2) inert

(3) extremely low background levels in the subsurface and the atmosphere

(4) non-toxic

(5) low solubility in water/brine

(6) non-flammable

(7) economical at quantities required

Historically, radioactive tracers, such as tritiated methane (CH3T), were used for subsurface injections (Ljosland et al., 1993). During the 1980's, however, interest in chemical gas tracers—particularly in halogenated compounds like SF_6—began to pique. Extensive laboratory studies led to several successful field deployments of SF_6 tracer (Langston and Shirer, 1985; Omoregie et al., 1988; Tang and Harker, 1991). These field studies showed that SF_6 could successfully be used as a conservative tracer for interwell tracer tests in several subsurface environments.

PFTs have been used in a wide variety of applications such as in atmospheric pollutant transport (Dietz, 1986), leak detection (Senum et al., 1997; Ghafurian et al., 1999; Heiser et al., 2005), and indoor air quality (Demokritou et al., 2002; Batterman et al., 2006). In subsurface applications, PFTs have been used for analyses of geothermal systems (Maxfield et al., 2005; Reimus et al., 2011), characterization of natural gas reservoirs (Ljosland, 1993) and partitioning interwell tracers to quantify light non-aqueous phase liquid (LNAPL) contamination (Jin et al., 1995; Whitley, 1997; Deeds et al., 2000).

Table 2-1: Chemical names and formulas for PFTs most commonly used in CCS monitoring

Tracer	**Chemical Name**	**Formula**
PDCB	perfluorodimethylcyclobutane	C_6F_{12}
PMCP	perfluoromethylcyclopentane	C_6F_{12}
PMCH	perfluoromethylcyclohexane	C_7F_{14}
o-PDCH	perfluoro-1,2,-dimethylcyclohexane	C_8F_{16}
PECH	perfluoroethylcyclohexane	C_8F_{16}
PTCH	perfluorotrimethylcyclohexane	C_9F_{18}

PFTs have also been used as tracers for enhanced oil recovery (EOR) projects, a technology related to CCS. Senum et al. (1992) used PFTs as part of a project to assess the viability of EOR by gas injection in the Naval Petroleum Reserve in California at Elk Hills. PFTs were co-injected with a gas into a reservoir and sampled at 18 sampling wells to qualitatively assess the extent of gas injection. Concurrently, Ljosland et al. (1993) deployed PFT at an EOR site at the Gullfaks field in the North Sea, noting PFT's low detection limits and previous atmospheric transport experiments as the two main

benefits of PFTs as tracers. Their study found that PFTs partitioned slightly into oil but were otherwise reliable tracers for interwell tracing.

Table 2-2: Historical usage of tracers for experimental CCS monitoring and verification projects. References: 1) Wells et al., 2007 2) Freifeld et al., 2005 3) Stalker et al., 2009 4) Hovorka et al., 2011

Year(s) deployed	Reservoir	Location	Operator	Reservoir Type	Tracers	Ref.
2002-2004	West Pearl Queen	SE New Mexico	NETL	Depleted oil & gas	PDCH, PTCH, PDCB	1
2004	Frio	TX Gulf Coast	BEG	Brine	PMCH, PTCH, PMCP, PDCH, SF_6, Kr	2
2008	Waarre "C"	Victoria, Australia	CO2CRC	Depleted natural gas	SF_6, Kr and CD_4	3
2010	Cranfield	SW Mississippi	BEG	Depleted oil & gas/ EOR	Kr, Xe, PFTs, SF_6	4

Tracer technology for CCS is an area of growing research with only a few full-scale pilot projects completed or underway. These projects differ from previous EOR applications because they seek to use tracers not only for interwell tracing and reservoir characterization but also for quantitative leak detection in the NSMZ. One of the noted publications (Wells et al., 2007) successfully estimated a leak rate from tracer flux to the NSMZ.

2.3 CHEMICAL BACKGROUND

2.3.1 Perfluorocarbons

Perfluorocarbons are totally fluorinated alkylcycloalkanes with low solubility in water and moderate vapor pressure (Dietz, 1986). PFTs have no biological toxicity (Chang et al., 1989; Varani et al., 1996). Six common cyclic PFTs are used in CCS tracing, described in Table 2-3 and pictured in Figure 2-1. Due to their large number of fluorine atoms, PFTs have a high affinity for electrons. This property makes PFTs one of the most sensitive compounds detected by electron capture detectors (ECD) (Dietz, 1986; Watson et al., 2007).

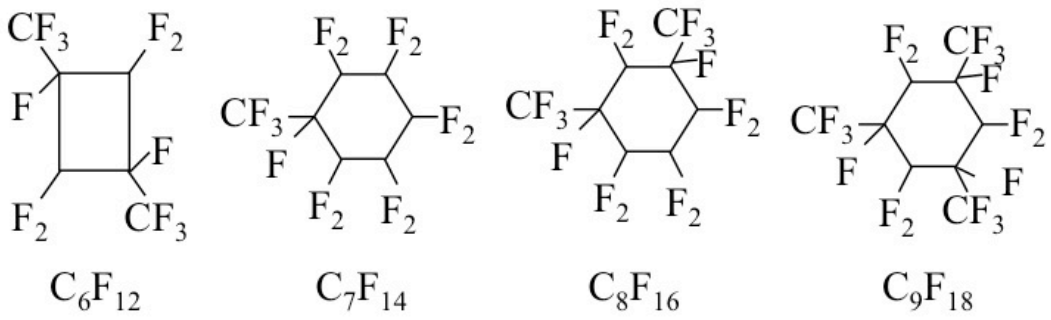

Figure 2-1: Perfluorocarbon tracers, adapted from Whitley, 1997.

Table 2-3: Chemical properties of PFTs. (Watson et al., 2007; Senum et al., 1992)

	[1]Molecular weight	[1]Boiling point	[2]Melting point	$^{2}T_c$	$^{2}P_c$	[2]Density at 20°C
	g mol^{-1}	°C			atm	g cm^{-3}
PDCB	300	45	-40	170.1	21.0	1.67
PMCP	300	48	-45	177.9	22.5	1.72
PMCH	350	76	-39	210.2	21.1	1.80
o-PDCH	400	102	-22	235.2	18.7	1.87
PECH	400	102	-60	234.1	18.7	1.77
PTCH	450	125	-56	257.5	17.2	1.90

2.3.2 Sulfur Hexafluoride

SF_6 is a halogenated compound with a long history as an environmental tracer. It is a nonflammable, nontoxic, stable gas and has almost entirely anthropogenic sources (Deeds et al., 2008; Rigby et al., 2010). It has a molecular weight of 146 g mol^{-1}, a boiling point of -64°C, a vapor pressure of 162.2 kJ kg^{-1}, a critical temperature of 45.5°C, and a critical pressure of 37 atm. It does not sorb onto organic matter or biodegrade (Busenberg and Plummer, 2000). The solubility for SF_6 has been determined to be 0.007 vol/vol in pure water at 20°C and 1 atm. However, SF_6 solubility is negatively correlated with salinity. Solubility decreases 25%-35% in seawater versus deionized water (Busenberg and Plummer, 2000). SF_6 has been used widely as a groundwater tracer (Busenberg and Plummer, 2000; Plummer et al., 2001; Gooddy et al., 2006), a tracer for ocean mixing (Ledwell et al., 1993; Sonnerup et al., 2013) and atmospheric mixing (Lovelock and Ferber, 1982; Levin and Hesshaimer, 1996).

2.3.3 Background Concentration

Both SF_6 and PFTs have low background concentrations. Studies have found atmospheric background concentrations of PFTs are in the low part per quadrillion range, growing at less than one part per quadrillion per year (Watson et al., 2007). SF_6 has an atmospheric concentration of 6.24-6.65 pmol mol^{-1} and is growing at a rate of 0.29 ± 0.02 pmol mol^{-1} yr^{-1} (Rigby et al., 2010).

2.3.4 Greenhouse Gases

Both PFTs and SF_6 are powerful greenhouse gases and have long atmospheric lifetimes, on the order of thousands of years (Bera et al., 2004; Watson and Sullivan, 2012). PFTs have a warming potential 10^3-10^4 as high as CO_2. At present, PFT concentrations in the atmosphere are not sufficiently high to cause significant warming and are not regulated by the Kyoto Protocol (Bera et al., 2004). The warming potential for SF_6 is 22,800 times that of CO_2 and has an atmospheric lifetime of 1935-3200 years (Busenberg and Plummer, 2000). It is regulated under the Kyoto Protocol (Rigby et al., 2010) as well as by the European Union (Regulation(EC) No 842/2006). The global warming potential for both tracers will certainly be a cause for concern as their use in CCS tracer testing matures.

2.4 GAS FLOW IN POROUS MEDIA

Here, I discuss processes that affect the transport of gases in dry porous media including advection, diffusion, dispersion, and adsorption. Each process is described with an emphasis on how it will alter the behavior of tracer breakthrough curves.

These phenomena are described in the context of a one-dimensional continuous flow column (flow parallel to the x-direction) that is packed with a homogenous porous media. In one dimensional column flow reactors, lateral transport perpendicular to the x-direction is assumed to be negligible. A non-reactive carrier gas flows at a continuous rate through the length of the column from the inlet (x=0) to the outlet (x=L), where L is the column length. At the beginning of the experiment (t=0), a finite volume of tracer concentration is injected at the inlet. This is analogous to, and modeled as, a pulse-style tracer injection. The tracer concentration is measured at x=L through time and presented in graphical form. The time at which the tracer reaches x=L is called the "breakthrough." This overall curve is called a breakthrough curve and it presents the change in tracer concentration at a certain distance away from the injection point as a function of time. This experimental model is analogous, albeit simplified, to a two-well tracer injection field test where a tracer is injected at one well and recovered at a second well over a period of time.

2.4.1 Advection

Advection is the transport of a substance in a fluid by the fluid's bulk motion. Advection is a controlled variable in the following experiments, quantified by measuring flow rate, Q, of the carrier gas (L^3T^{-1}). Flow rate is used to calculate average flow velocity through the column, which is the velocity of the fluid as it crosses through a unit cross sectional area of pore space (Fetter, 1999). The equation to calculate average flow velocity from flow rate is:

$$v = \frac{Q}{A\phi} \qquad \textbf{Eq. 3.1}$$

where v is average velocity [LT^{-1}], A is the cross sectional area of the column [L^2] and ϕ is porosity [-]. This is an average velocity through the column and does not represent actual velocities at specific locations through the column, which vary as a result of differential pore structures.

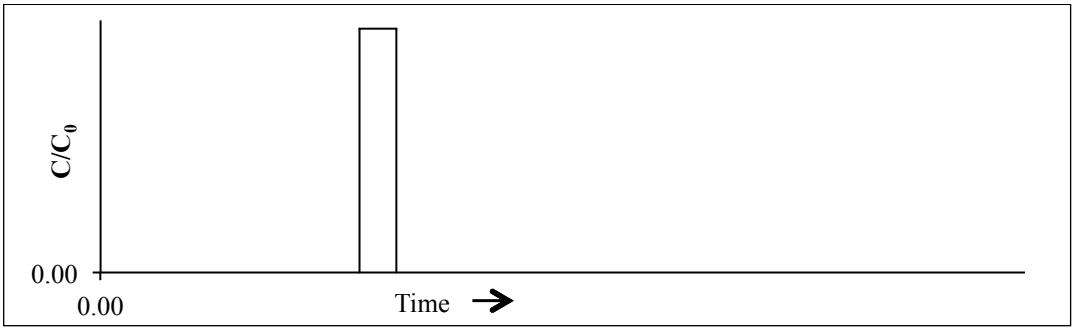

Figure 2-2: Breakthrough curve of tracer with a pulse injection under advective flow alone

The one-dimensional advective transport equation to describe gas transport due to advection-only flow is

$$\frac{\partial C}{\partial t} = -v\frac{\partial C}{\partial x} \qquad \textbf{Eq. 3.2}$$

where C is concentration [M L^{-3}]. The solution to this equation yields a symmetric breakthrough curve with a sharp front, as illustrated in Figure 3-1. The analytical solution to this equation shows that:

$$C(x,t) = F(x - vt) \qquad \textbf{Eq. 3.3}$$

In this simple case, where only advection at a constant velocity controls tracer flow, the concentration profile moves through space and the shape of the concentration profile does not change. The width of the peak is controlled by the volume of the injection source and injection time. This can be modeled as a Dirac delta function where the width of the peak is zero with respect to time. The analytical model applied in this study assumes a tracer injection analogous to a Dirac delta function. The Dirac delta function is further described in Section 4.8.

2.4.2 Dispersion

The term dispersion couples the effects of two different processes: mechanical dispersion and diffusion (Fetter, 1999). In practice, separating the effects of these two processes is difficult and often impossible. The physical difference between mechanical dispersion and diffusion is that dispersion is the result of advection, or bulk flow of gas, whereas diffusion is dependent on the concentration gradient, independent of advection and will occur in non-flowing fluids (Fetter, 1999).

a. Mechanical dispersion

In any system with bulk flow, some particles move at velocities greater than the mean flow velocity, while others move at velocities less than the mean flow velocity. This range of velocities can be attributed to two main forces. First, friction on the walls of pores causes molecules in the pore center to move at higher velocities than those closer to the pore wall. The maximum velocity in the center of the pore depends on the pore size and shape as well as flow rate (Bear, 1979). Second, velocity is affected by the topology of the pore network. Molecules moving in the same net direction (parallel to the x-direction, for example) may take many different flowpaths, some of which are longer or shorter than average (Bear, 1979; Fetter, 1999). The net result of these longer pathways is an increase in tortuosity, or the deviation of flow paths from a straight line. Tortuosity is a property inherent in the porous media, independent of flow parameters. Mechanical dispersion increases with average linear velocity.

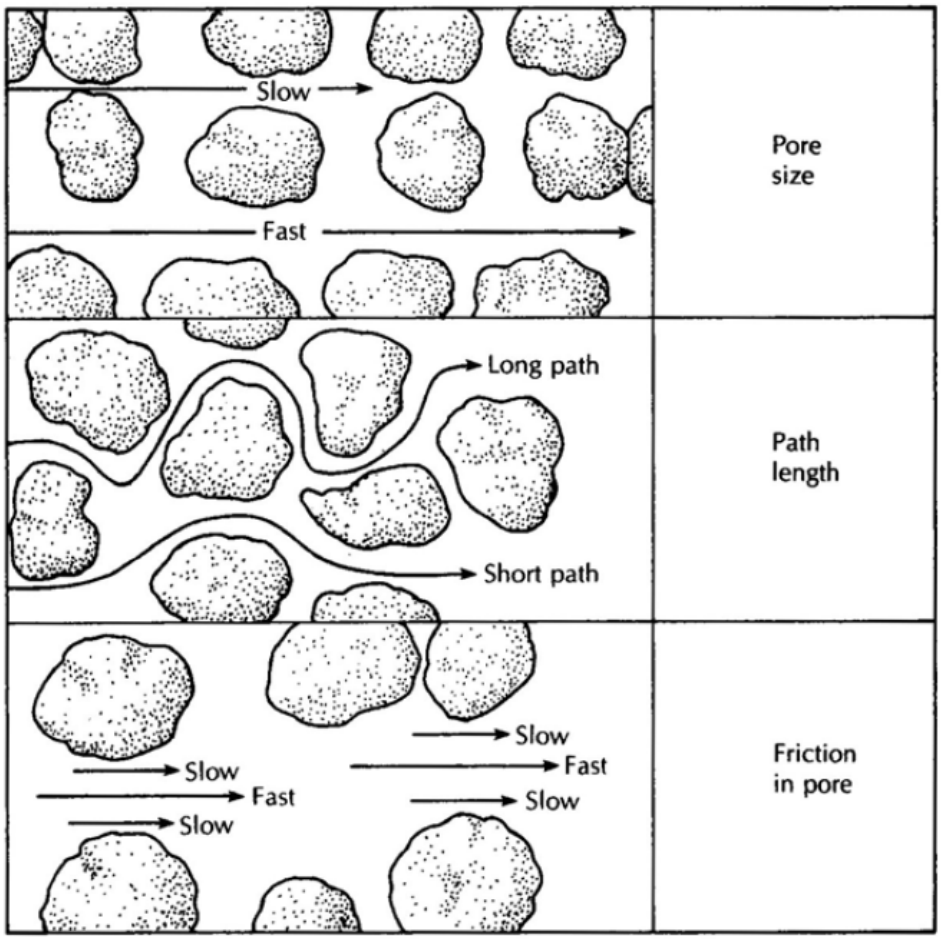

Figure 2-2: Factors contributing to longitudinal hydrodynamic dispersion (Fetter, 1994, p. 456)

As a result of mechanical dispersion, the finite tracer volume spreads longitudinally in both the direction of average flow and the direction opposite average flow. Therefore, the initial breakthrough of the tracer occurs more quickly than would be predicted if the fluid was subject to advection alone. Advection plus mechanical dispersion will cause spreading in the tracer breakthrough and result in a Gaussian breakthrough curve with symmetric tails (see Figure 2-3).

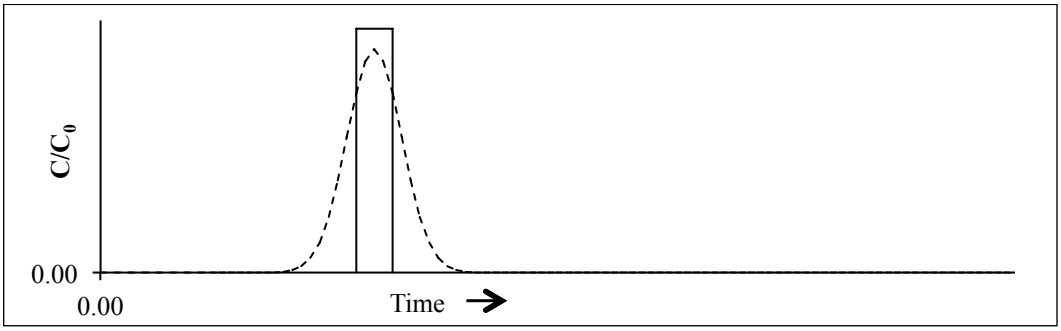

Figure 2-3: Breakthrough curve of tracer with a pulse injection under advective flow alone (solid line) and advective flow plus dispersion (dashed line).

Mechanical dispersion is described mathematically by the coefficient of mechanical dispersion:

$$Coefficient\ of\ mechanical\ dispersion = \alpha_L v \qquad \textbf{Eq. 3.4}$$

where v is the average linear velocity [LT^{-1}] and α_L is a the apparent longitudinal dynamic dispersivity [L], a property specific to each porous medium. The subscript "L" indicates that dispersivity is in the longitudinal direction. For more complex flow patterns in two and three directions, each direction will have its own dispersivity. In the case described here, dispersivity parallel to the flow direction (the x-direction) is the only effect considered.

Neuman (1990) gives a relationship between the length of the flow path (or column length) and the apparent longitudinal dynamic dispersivity, α_L, which applies to flow paths less than 3500 m:

$$\alpha_L = 0.0175 L^{1.46} \qquad \textbf{Eq. 3.5}$$

where L is the length of the flow path in meters. When experimental simulations fit this criterion, the α_L can be determined.

b. Diffusion

Diffusion is a result of random (Brownian) molecular movement leading to mixing of fluids in the absence of bulk flow (Fetter, 1994). Diffusion causes mixing of fluids from areas of high to low concentrations. The rate of diffusion is affected by, among other things (e.g. temperature and pressure), the concentration gradient, such that diffusion reaches equilibrium when the fluid is of uniform concentration. Fick's first law of diffusion expresses the mass of a tracer diffusing through a given area in the presence of a concentration gradient:

$$F = -D_{ij}\frac{dC}{dx} \qquad \textbf{Eq. 3.6}$$

where F is the flux of tracer [M L^{-2} T^{-1}], D_{ij} is the diffusion coefficient for gas tracer i into carrier gas j [L^2 T^{-1}], C is solute concentration [M L^{-3}], and dC/Cx is the concentration gradient [M L^{-3} L^{-3}]. The negative sign indicates movement from high to low concentration areas. Fick's second law describes diffusion in a system with changing concentrations:

$$\frac{\partial C}{\partial t} = D_{ij}\frac{\partial^2 C}{\partial x^2} \qquad \textbf{Eq. 3.7}$$

The diffusion coefficient is specific to a particular tracer into a particular carrier gas. Typically, the binary diffusion coefficients between two gases can be accurately

calculated with respect to either temperature or pressure. The Fuller Equation (Fuller et al., 1966) is one empirical method used to calculate the binary diffusion coefficients between two gases. The Fuller Equation is a least squares regression fit to empirical datasets and is dependent on temperature, pressure, atomic mass and diffusion volumes of each diffusing species. The Fuller Equation is as follows:

$$D_{ij} = \frac{1\times10^{-3}T^{1.75}\left(1/M_i + 1/M_j\right)^{1/2}}{p\left[\left(\sum_i V_i\right)^{1/3} + \left(\sum_j V_j\right)^{1/3}\right]^2} \qquad \textbf{Eq. 3.8}$$

where T is temperature in Kelvin, $M_i$and M_j are the molecular weight of components *i* and *j*, respectively, in grams, p is pressure in atmospheres and $\sum_i V_i$ and $\sum_j V_j$ are the sum of the diffusion volume for components *i* and *j,* respectively. The diffusion volumes are empirically determined.

The diffusion coefficient calculated above holds true in a domain with no porous media. In porous media, diffusion is not as efficient due to tortuosity. Molecules must take longer pathways through pores and pore throats. To account for tortuosity, a new diffusion coefficient, the effective diffusion coefficient, D* is used:

$$D^* = \omega D_{ij} \qquad \textbf{Eq. 3.9}$$

where ω is a tortuosity coefficient with a value between zero and one found experimentally. In most geologic media, ω ranges from 0.001 to 0.5. In sand, ω is about 0.7 (Fetter, 1999).

c. Hydrodynamic Dispersion

Because mechanical dispersion and diffusion cannot be separated in practice, they are combined into one parameter: the hydrodynamic dispersion coefficient, D_L (Bear, 1979; Fetter, 1999). The subscript indicates longitudinal dispersion, parallel to flow. The hydrodynamic dispersion coefficient, D_L, can be expressed as

$$D_L = \alpha_L v + D^* \qquad \textbf{Eq. 3.10}$$

Mechanical dispersion is a result of advection and therefore does not occur when flow velocity is zero. Diffusion, on the other hand, is dependent on time and independent of flow and occurs even if flow velocity is zero. Therefore, influence of diffusion is strongest at low flow velocities (Bear, 1979).

2.4.3 Peak Tailing and the Péclet number

Breakthrough curves on real geologic media are rarely Gaussian (i.e. a symmetric shaped [bell] curve). Figure 2-4 shows several examples of non-Gaussian breakthrough curves in real geologic media. Breakthrough curve skewness is a function of many parameters including sorption-desorption kinetics, two-site sorption, carrier gas flow rate and diffusivity (Lenhoff, 1987; Hsu and Chen, 1987). The latter two properties are combined to form the dimensionless Péclet number, *Pe*.

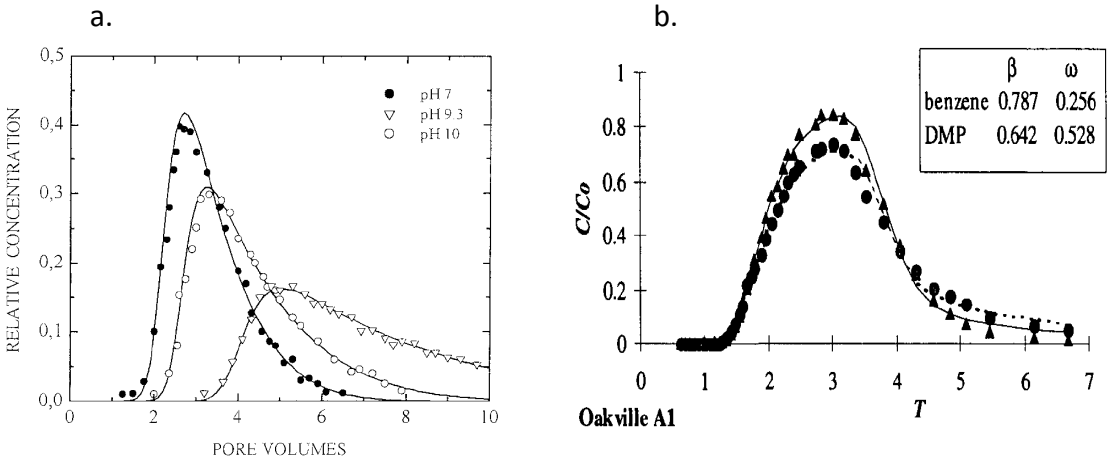

Figure 2-4: Examples of non-Guassian breakthrough curves on real geologic media. a) Boron breakthrough on 3 clean sand columns (Communar et al., 2004) and b) Benzene (triangles) and dimethylphthalate (circles) breakthrough curves on soil (Maraqa et al., 1998)

Peak skewness is directly proportional to Pe and, thus, inversely proportional to D_{ij}. In column studies, Pe is calculated as:

$$Pe = \frac{\nu d}{D_{ij}} \qquad \textbf{Eq. 3.11}$$

or as

$$Pe = \frac{\nu L}{D_L} \qquad \textbf{Eq. 3.12}$$

where d is the average grain diameter. The Péclet number can be thought of as the relative contribution of tracer transport by advection and dispersion versus the contribution of tracer transport by diffusion.

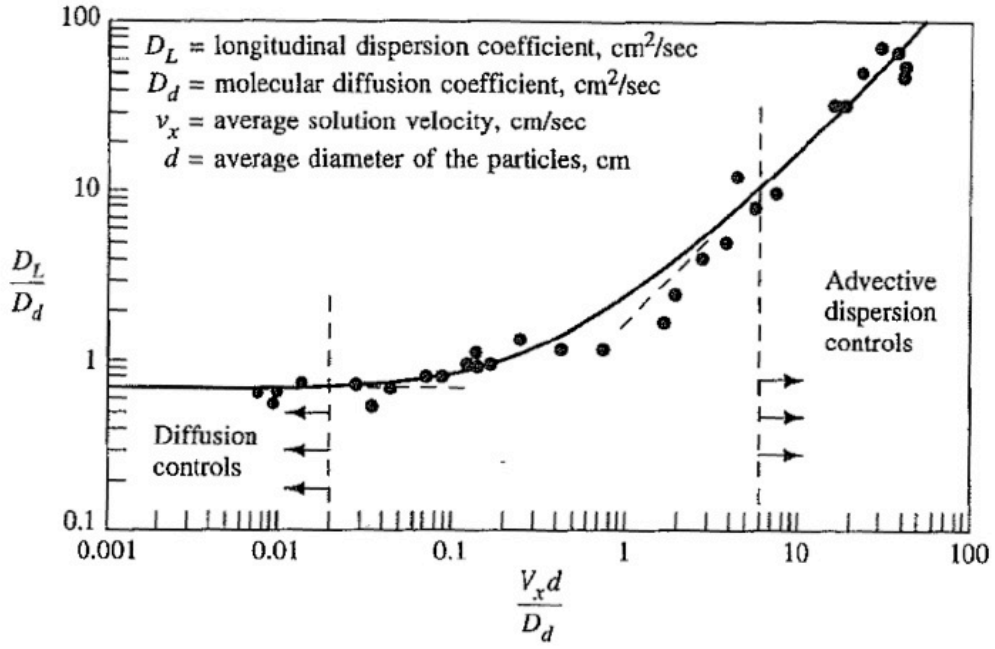

Figure 2-5: Graph of dimensionless dispersion coefficients vs Péclet number where *Pe* is as defined in Equation 3.11 (Perkins and Johnston, 1963)

If D_L is known, the ratio of hydrodynamic dispersion to diffusion, $\frac{D_L}{D_{ij}}$, can be used to describe the relative contribution of advection/dispersion and diffusion to transport. Such a relationship can be seen in Figure 2-5, which shows the results of transport experiments on a sand column (Perkins and Johnston, 1963). At low flow velocities, transport is dominated by diffusion and, in sand columns, $\frac{D_L}{D_{ij}}$<0.4. A transition zone (0.4<$\frac{D_L}{D_{ij}}$<6) exists where the effects of diffusion and advection are about equal. At $\frac{D_L}{D_{ij}}$>6, advection/dispersion controls flow, D_{ij} can be ignored, and $D_L = \alpha_L v$ in the advection-dispersion equations.

2.5.4. Retardation

Tracers can be broadly divided into two categories: conservative and reactive. Tracers that do not react with the soil or porous media and do not undergo biological or radioactive decay are conservative. Noble gases, for example, are often used as conservative gas tracers and SF_6 is commonly considered a conservative tracer in near-surface environments (Santella et al., 2003). Conservative tracers are transported at the same rate as a non-reactive carrier fluid. For example, N_2 is a commonly used nonreactive carrier fluid. However, it should be noted, in the context of CCS, CO_2 is the carrier fluid and it is reactive.

Reactive tracers, by contrast, can be partitioned into liquid phases, sorbed onto surfaces of mineral grains, sorbed by organic carbon, precipitate, undergo biotic or abiotic degradation, or participate in chemical reactions (Fetter, 1999). As a result, the reactive tracer will be transported through the porous medium slower than the bulk flow of the carrier fluid, an effect called retardation. A tracer may be non-reactive but undergo a phase change, or precipitation of a liquid, which may cause retardation as well. Unless the tracer is biodegraded, radioactively decayed, or precipitated, the total mass of the tracer in the system will not decrease.

Sorption processes include adsorption, chemisorption, absorption, and ion exchange. Adsorption is the process by which the adsorbate, the chemical being adsorbed, clings to a solid surface. Cation exchange occurs when a chemical is attracted

to the surface of an oppositely-charged mineral by electrostatic forces. Clays provide negatively charged sites, for example, whereas iron and aluminum oxides can provide positively-charged sites. Chemisorption occurs when a chemical is incorporated onto a solid surface by a chemical reaction. Absorption is the process by which a chemical is incorporated into the mineral, rather than on the mineral surface. In addition to sorption processes, chemicals can be partitioned into liquid phases within the porous medium.

2.4.5 Adsorption Isotherms

Sorption process can be described using adsorption isotherms. The adsorption isotherm is a common way to characterize and potentially identify adsorption processes. Understanding the adsorption process is important for predicting the fate of sorbing gases in the vadose zone and emission rates from the vadose zone to the atmosphere. Typically, adsorption isotherms either describe (1) the mass of adsorbate adsorbed as a function of pressure at a given temperature or (2) the mass of adsorbate adsorbed as a function of concentration of adsorbate at a given temperature. The former type can be used with nitrogen as the adsorbate to determine surface area of porous materials. The latter type, described below, can be used to describe the adsorption of a non-conservative tracer onto a specific porous media.

Broadly, isotherms can be described by linear or non-linear models. Non-linear sorption isotherms are more common in natural systems. The three most common types of non-linear sorption isotherms are Freundlich, Langmuir and the BET (Brunauer,

Emmet and Teller) models. Among other things, these models differ in their assumptions about maximum adsorption capacity. Freundlich assumes that the amount of gas adsorbed increases without limit. Langmuir assumes that maximum adsorption occurs when a monolayer or sorbate is formed. The BET Model incorporates the idea of multiple adsorption layers. The method of moments and advection dispersion model described in Section 4.8 assumes a linear adsorption model, which may be sufficient for the purpose of identifying adsorbing gases in simple flow through experiments.

Following the work of Buergisser et al. (1993), adsorption isotherms can be simplified as linear, convex or concave and determined by using a step injection of tracer onto a column. Figure 2-6 shows tracer breakthrough curves on the bottom (concentration of tracer [C(t)] versus normalized time [t/t_0]) and their corresponding isotherms on the top (adsorbed concentration [C_a] versus total concentration [C]). The isotherms are derived by integrating the desorption branch of the breakthrough curve, which is the right tail in the case of a convex isotherm and the left tail in the case of a concave isotherm.

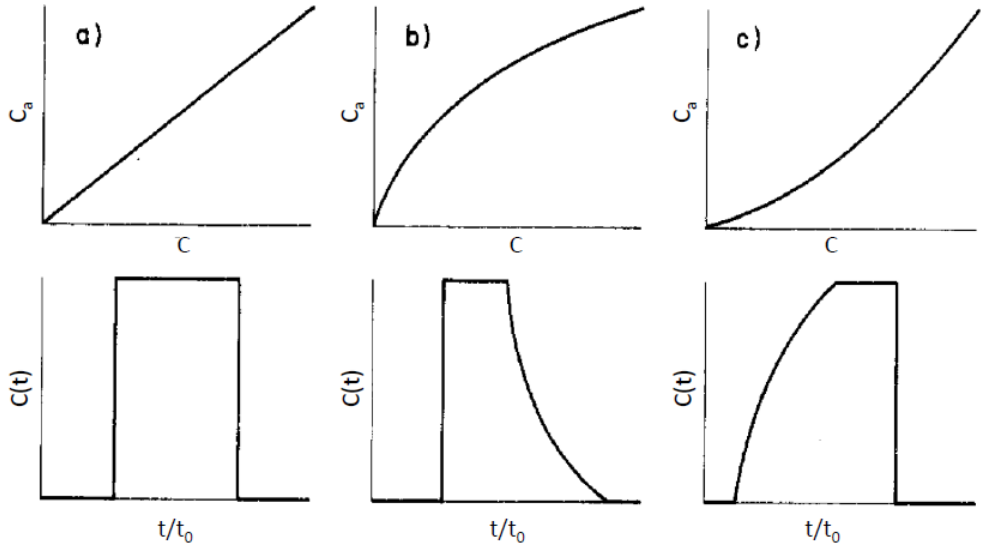

Figure 2-6: Schematic representation of the breakthrough curves on packed columns (bottom) and their corresponding adsorption isotherms (top). The column breakthrough curve for a step injection without dispersion is shown for a) linear, b) convex and c) concave isotherms (Buergisser et al., 1993)

This is a unique approach and convenient to perform given available experimental setup; most adsorption isotherms are determined using batch reactors or diffusion experiments. The experiments herein will qualitatively determine whether PFT follows a linear or nonlinear isotherm in a packed column as well as test the usefulness of adsorption isotherms based on the packed column method.

2.4.6 Batch vs. Column Experiments

Column experiments have been used in environmental sciences for over three centuries to test hydrologic properties of soils and fluid flow, the most famous example being Darcy's groundbreaking work describing the transport of fluids through porous media (Darcy, 1856; Lewis and Sjöstrom, 2010). In the last few decades, column

experiments have been expanded to test solute transport models (Klein et al., 1997; Stoessell, 1999), fate and mobility of contaminants in soil (Artinger et al., 1998; Mibus et al., 2007), and they have been shown to be effective in determining retardation factors and adsorption isotherms (Maraqa et al., 1998). Historically, however, both batch and column experiments have been used to determine retardation factors and adsorption isotherms of gases or solutes in porous media (Buergisser et al., 1993; Maraqa et al., 1998; Artinger et al., 1998). There are several reasons why column experiments are chosen to evaluate PFT and SF_6.

Batch experiments involve adding a chemical (sorbate) of interest to a porous media (sorbent) in a closed system and measuring the concentration of sorbate in the headspace or in aqueous solution, depending on the specificities of the experiment. Column experiments, also known as flow-through experiments, are performed by packing a column with a porous media, inducing a flow of carrier gas or aqueous solution, injecting the sorbate of interest, and measuring the concentration of sorbate in the effluent.

Several discussions of the advantages and disadvantages of column and batch experiments have been published (Jackson et al., 1984; Kool et al., 1989; Buergisser et al., 1993; Grolimund et al., 1995; Maraqa et al., 1998). In general, batch experiments are noted for their ease of operation and low experimental variation. They are advantageous because they allow direct and independent measurements of specific parameters and have

a long history of use in environmental applications (Kool et al., 1989). However, batch experiments have been found to be susceptible to several systematic errors. For example, mechanical shaking during the experiment may induce physical changes in the sorbate (Schweich et al., 1982) and the separation of high molecular weight molecules from the sorbent is not possible with common shaking procedures, resulting in poor estimates of the equilibrium coefficient (Buergisser et al., 1993). These problems result in two common difficulties with batch experiments, particularly in the case of weak adsorption: 1) overestimates of retardation coefficient (Maraqa et al., 1998) and 2) the particle concentration effect (the equilibrium coefficient appears dependent on the solid-to-solution ratio though it is, in fact, independent) (Gschwend and Wu, 1985; Buergisser et al., 1993; Grolimund et al., 1995). The equilibrium coefficient is the ratio of the concentration of the sorbate adsorbed onto the porous media to the concentration of the sorbate in the carrier gas. It is discussed in Section 3.7.2.

Column experiments are noted for their reduced experimentation time and better (though not perfect) approximation of field conditions (Jackson et al., 1984). They have the advantage of determining nonlinear isotherms, which are common in soils and aquifer materials, more easily than batch experiments (Buergisser et al., 1993). Another good feature of column experiments is the ability to estimate multiple parameters simultaneously: the pore volume, Péclet number, dispersion coefficient, adsorption coefficient, as well as retardation factors. The main disadvantage of column experiments

is the variability of results, particularly when an undisturbed (natural) soil is used as the packing material. Results from column experiments using heterogeneous soil could be affected by a host of issues, from preferential flow paths, to flow into/from aggregates, etc., leading to substantial variability in breakthrough curves. This is not problematic for the experiments conducted herein because the packing material is re-packed (not natural). Another disadvantage of column experiments is that the experiment must obey the local equilibrium assumption, or instantaneous adsorption, for the determination of adsorption isotherms (Buergisser et al., 1993; Maraqa et al., 1998).

Discrepancies of retardation factors between batch and column experiments are common (MacIntyre and Stauffer, 1988; Lion et al., 1990; Piatt et al., 1996). Though many causes are considered and several are listed above, the true cause of difference in retardation factor between the two techniques remains unclear (Maraqa et al., 1998). Therefore, to minimize the risk of obtaining poor estimates of the retardation factor estimation, the specific conditions of the experiment at hand must be considered.

This study uses column experiments. These experiments are designed to minimize experimentation time, provide maximum data on both the adsorption and flow processes, and provide framework to explore nonlinear isotherms. Loose packing material and a well-designed packing technique are used to minimize problems with reproducibility and preferential flow paths. The following sections discuss the porous

media, packing method, and experimental setup used to produce breakthrough curves for tracers.

3. Experimental Setup and Methods

3.1 Porous Media

The goals of this project are to identify under what conditions PFTs behave conservatively with respect to SF_6 and to quantify the retardation factors for conditions that produce non-conservative behavior. With this end in mind, five different packing materials are chosen. These media cover a range of conditions from the most simplistic (acid-washed silica beads) and increasing in complexity (quartz sand) to the most complex (soil samples and illite). The soils included one organic-rich sediment from Colombia (C-soil) and one organic-poor sediment from Brazil (B-soil).

Both silica beads and quartz sand are included because they have the same mineralogy but different surface area and particle size distribution. Differences in breakthrough curves between the two can indicate how grain size and surface area affect retention times and peak shape. Illite is included because it is one of the most adsorptive materials and clays are common in the NSMZ.

The soils were chosen primarily to investigate the influence of soil organic matter on PFT retardation. The soils have very different grain size distribution (Section 4.2.1) and total organic carbon (TOC) content (Section 4.2.2). Differences in grain size distribution may complicate the analysis of the absorptiveness of organics. The B-soil also demonstrates the practical applicability of column tracer tests for CO_2 injection

experiments. This soil was sampled from a near-surface CO_2 injection project in southern Brazil where PFT tracers are being used as a gas tracer. These experiments will help inform the analysis of PFT data from that site.

The C-soil was collected in Colombia (Lat: 4.56466 and Lon: -73.97177) at an elevation of 3068 m and a depth of 80 cm. The sampling site is humid, with a mean annual precipitation of 1402 mm yr^{-1} and mean annual temperature of 11.37 ˚C. The B-soil was collected in Brazil (Lat: -27.67666, Long: -48.54022) at the site of a shallow CO_2 injection experiment by the the Pontifical Catholic University of Rio Grande do Sul's Centro de Excelência em Pesquisa e Inovação sobre Petróleo, Recursos Minerais e Armazenamento de Carbono (PUCRs CEPAC). Elevation of the site is 7 m but the depth was not reported. The climate is humid subtropical with a mean annual precipitation of 1521 mm yr^{-1} and a mean annual temperature of 20.62 ˚C.

The techniques used to prepare packing material are as follows:

Silica beads: Silica beads of size 0.211-0.152 mm (70-100 US Sieve) were purchased from Sigma Aldrich. The beads were acid-washed in 5 M nitric acid followed by several rinses in deonized and then double deonized water.

Quartz Sand: Quartz sand was sieved to 100-250 micron before packing.

Illite*:* Illite is in aggregate form. It is not sieved.

***Colombia soil*:** The Colombia sediment (C-soil) was dried, crushed and sieved 0.422-0.125 mm (40-120 US sieve). Larger twigs and root particles were removed before packing.

Brazil soil: Sediment from Brazil (B-soil) was rinsed three times in de-ionized water, dried and packed without sieving.

3.2 MEDIA ANALYSIS

3.2.1 Particle Size Distribution and Surface Area

Particle size distribution was measured in wet suspension using a Malvern Mastersizer 3000 laser diffraction particle size analyzer. The media was not disaggregated before analysis.

Surface area analysis for the C-soil and illite were performed using an Autosorb-iQ-MP instrument (Quantachrome Instruments) equipped with a vacuum capable of reaching 5×10^{-7} Pa. Sample masses of at least 90 mg were placed into 6mm stem quartz sample cells and degassed for 8 hours at 250 °C under vacuum. Nitrogen at 77K was used as the probe gas for all experiments. Surface areas were calculated using the best linear range between 0.05-0.3 P/Po of N_2 soprtion, with a minimum of 5 points used in the BET analysis.

For silica beads and quartz sand, the surface area is too low to be analyzed using this method. The B-soil was also not analyzed by the BET analyzer. For these packing

materials, all grains are assumed to be spherical and the equation for specific surface area is:

$$\mathrm{SSA} = \frac{4\pi r^2}{\mathrm{m}} \qquad \textbf{Eq. 3.1}$$

where r is the radius of the average grain size [L] and m is the mass of a grain with the same radius [M]. Density is assumed to be 2.65 g cm^{-3} (Gaines et al., 1997). The assumption that all grains are spherical is valid for silica beads but underestimates the surface area of the quartz sand and the B-soil. The mean grain size for silica beads is 161.0 μm, for quartz sand it is 174.0 μm and for B-soil it is 184.23 μm.

3.2.2 Mineralogy and Organic Carbon

Both soils were analyzed for mineralogy using X-ray diffraction. Loss on ignition method (LOI) from the U.S. EPA report, Methods for the Determination of Total Organic Carbon (TOC) in Soils and Sediment is used to measure TOC (Schumacher, 2002). LOI is a semi-quantitative method, based on the indiscriminate removal of all organic matter from the sample and gravimetric determination of weight loss. The process is as follows:

1. Known weight of dry soil placed in ceramic crucible
2. Sample is heated to 375°C for ~12 hours
3. Sample is cooled and weighed

Total organic content is calculated as:

$$TOC = \frac{M_i - M_f}{M_i} x100\% \qquad \textbf{Eq. 3.2}$$

where M_i and M_f are the mass of the sample before and after heating, respectively.

3.3 COLUMN PACKING

Column packing is a very important aspect of the experimental design and there have been many discussions of various packing methods for both saturated and unsaturated column experiments (Lewis and Sjöstrom, 2010; Koestel et al., 2012). Improper column packing can lead to layering or creation of preferential flow paths, which would affect transport behaviors. Thus, the goal of packing is to create a homogenous column of packing material that minimizes the creation of preferential flow paths or other zones of variable properties. Many different methods have been reported for different conditions of the material: dry or damp packing (Bégin et al., 2003; Darnault et al., 2004), wet packing (Nelson et al., 1999), and slurry packing (Jin et al., 1997).

Because the following experiments are run under dry conditions, the columns are packed with dry sediment, which has been shown to produce satisfactory results using a variety of methods (Whitley et al., 1999; Communar et al., 2004; Darnault et al., 2004). The method used in the following experiments is similar to those described by Whitley et al. (1999) and Darnault et al. (2004). Stainless steel columns (0.45-1.02 cm inner diameter and 50-100 cm length [see Table 4-1]) were washed with dichloromethane and fitted with a Swagelock reducing union packed with a small amount of quartz wool to prevent particulates from entering or exiting the column. The columns were kept vertical with the bottom end of a column resting on a vortexer cup head. The column is vibrated

while packing to encourage compaction of packing material while the material is poured slowly through a funnel into the column. When packing material reached the top of the column, vibrations were stopped and the column was fitted with another Swagelock end fitting packed with quartz wool.

3.4 POROSITY MEASUREMENT

For media with a known density, porosity of the column can be measured by simply weighing the column before and after it is packed. To do so, the volume of packing media is calculated as:

$$V_m = \frac{m_p - m_e}{\rho_m} \qquad \textbf{Eq. 3.3}$$

where V_m is the volume of packing media [L^3], m_p is the mass of the packed column [M], m_e is the mass of the empty column, and ρ_m is the density of the packing media [ML^{-3}]. Then, the porosity is simply:

$$\phi = \frac{V_m}{V_t} \qquad \textbf{Eq. 3.4}$$

and the pore volume is:

$$V_p = V_t - V_m \qquad \textbf{Eq. 3.5}$$

where V_t is the total volume of the column. V_t is calculated from the inner diameter and length of the tube.

Note that this method does not work for media of unknown density. For the following experiments, the porosity of silica beads and quartz sand were calculated this way, assuming a density of 2.65 g cm^{-3} for SiO_2 (Klein and Dutrow, 2008). Illite will have a porosity calculated assuming a density of 2.75 g cm^{-3}(Gaines et al., 1997).

3.5 EXPERIMENTAL PROCEDURES

The procedure for conducting column experiments consists of several steps, described below. All pulse injection experiments are run in triplicate.

3.5.1 Experimental Setup

The generalized experimental setup for a pulse injection can be seen in Figure 3-1.

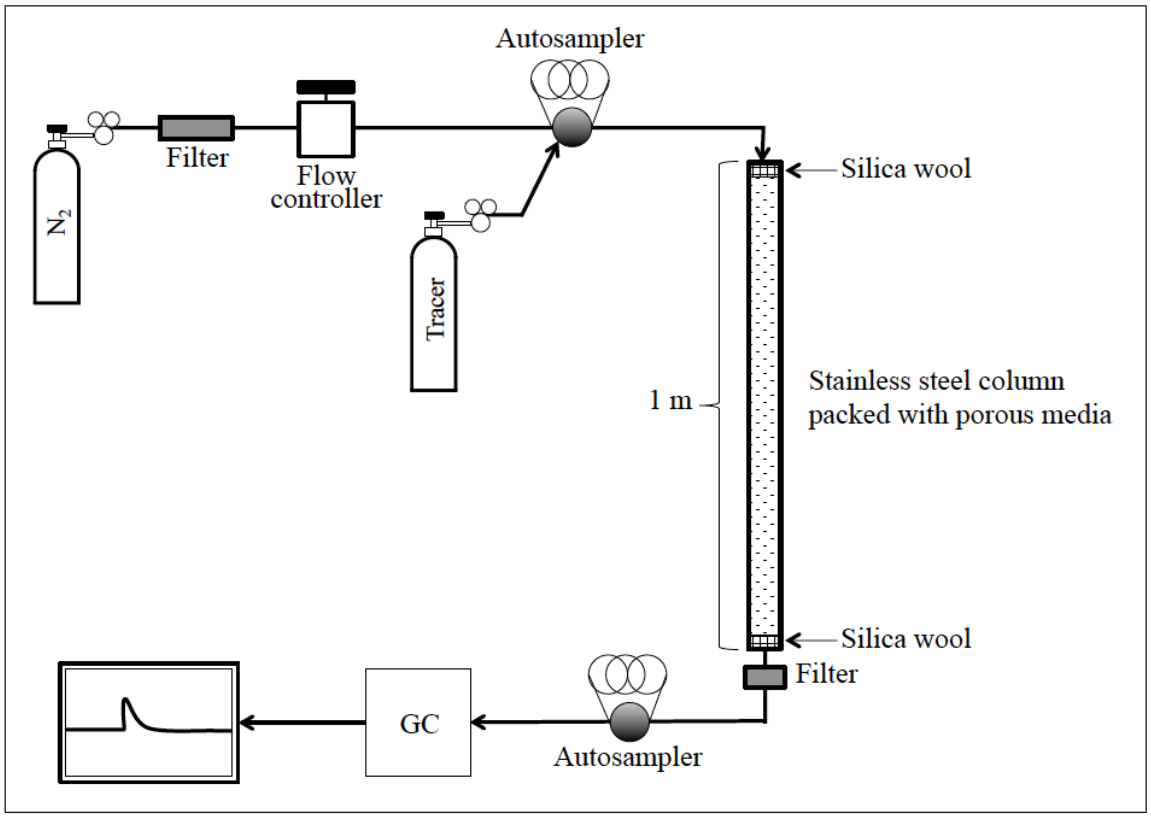

Figure 3-1: Experimental setup for column flow-through experiments

The packed column is connected to the carrier gas (ultra high purity N_2) and tracer via a 6-port autosampler (model EC26WE, Valco). A low flow controller (model MC-5SCCM-D/5M, Alicat Scientific) maintains carrier flow velocity. Silica wool is packed on both upstream and downstream ends of the column to maintain porous media consolidation and to prevent outflow of porous media to gas chromatograph. A stainless steel Swagelock welded particulate filter with a 7 micron pore size on the downstream end of the column safeguards against particulates entering GC. A second 6-port autosampler samples column effluent every 2-3 minutes, depending on the GC setup. The GC output is in the form of a chromatographic peak. For a pulse injection, the flow

controller is positioned upstream of the autosampler, as pictured. For a step injection, the flow controller is positioned downstream of the autosampler.

Table 3-1: Summary of column properties relevant to calculating flow properties. Note that there is a dead volume of ~2.3 mL on the columns and this is not reflected in the porosity measurements here.

	Packing material	**Length** ***cm***	**Inner diameter** ***cm***	**Cross sectional area** ***cm^2***	**Flow rate** ***$mL\ min^{-1}$***
A	Silica beads	100	1.02	0.82	1.25
B	Quartz sand	100	0.45	0.16	0.50
C	Illite	51	0.45	0.16	1.00
D	C-Soil	100	0.77	0.47	1.00
E	B-Soil	61	0.45	0.16	0.5 0

Table 3-2: Summary of Péclet numbers for each column. Tortuosity, ω, is estimated as 0.5 for all columns. D^*_{PMCP} is 0.025 $cm^2\ sec^{-1}$ and D^*_{SF6} is 0.050 $cm^2\ sec^{-1}$.

	Pe_{PMCP}	**Pe_{SF6}**	**Pe_{PMCP}**	**Pe_{SF6}**
	$\frac{vd}{D_d}$		$\frac{vL}{D_L}$	
Silica Beads	0.025	0.012	13.15	13.15
Quartz Sand	0.034	0.017	16.72	16.72
Illite	0.109	0.056	6.09	6.09
C-soil	0.100	0.051	22.02	22.02
B-Soil	0.019	0.010	2.71	2.71

3.5.2 Column preparation:

After porous media is prepared and column is packed according to steps described above, the column is attached to a flow of ultra-high purity, dry nitrogen gas. The low flow controller maintains steady carrier gas flow (see Table 4-1 for flow rate used in each experiment). The column is allowed to equilibrate and dry for ~24 hours. The column is leak tested using Snoop® Liquid Leak Detector. After drying, effluent of the column is tested to determine that background levels of tracer are sufficiently low (below detection limits).

The choice of flow rate for each experiment depends on the dimensions of the column, breakthrough time of tracer, and GC analysis time (1-2 minutes). The GC analysis time is determined by the retention time of the tracer in the GC column. The goal is to achieve a flow slow enough to capture the breakthrough of the tracer with as many data points as possible while minimizing experimental run time. The appropriate rate can be estimated by modeling tracer breakthrough curves but simple trial-and-error is usually necessary as well.

3.5.3 Tracer injection: Step vs. Pulse injection

Two different types of tracer injection were used in the following experiments: Pulse injection and step injection. The procedure for both injections is described and illustrated below (Figure 3-2).

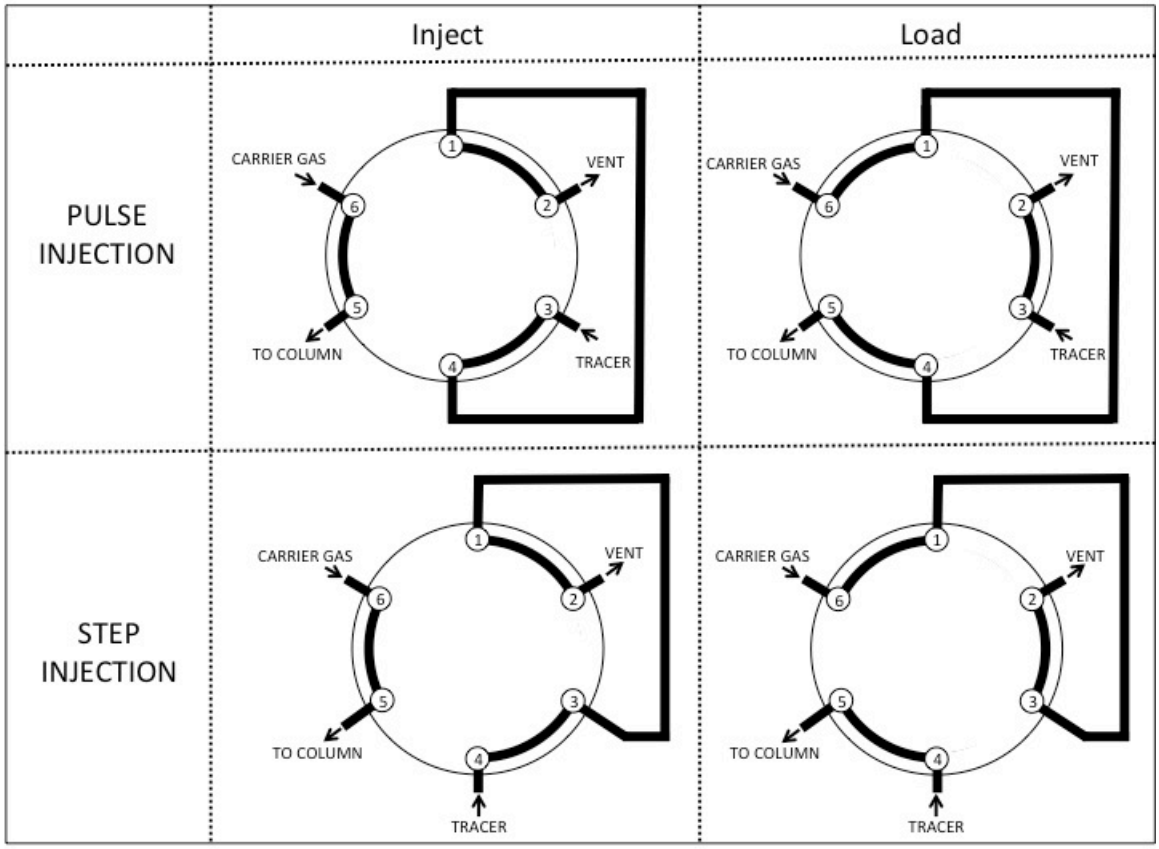

Figure 3-2: 6-port valve positions for both pulse and step injections

The first method is for a pulse injection of tracer. At the upstream end of the column, a 6-port automated sampling valve with a 100 μL sample loop is attached to a pressurized tank or gas bag of tracer at a desired concentration. Sample loop is flushed with tracer at a slow flow rate. After several seconds of flushing, the sample loop is filled with tracer. Noting time of injection, the 6-port valve is switched from "Inject" to "Load" position. The loop is flushed with carrier gas and injected onto the column. Concentration of tracer in gas eluted from the end of the column is monitored periodically.

The second method is for a step injection of tracer. For a step injection, the 6-port automated sampling valve is plumbed differently (see Figure 3-2) where the flow controller is positioned downstream of the sampling valve so that flow of tracer is controlled. The tracer line is allowed to flush for several seconds. Noting the time of injection, the 6-port valve is switched from "Inject" to "Load" position and the flow onto the column is thus switched from N_2 to tracer. Once the normalized tracer concentration equals 1 ($C=C_0$), the flow is switched back to the "Inject" position.

The methods result in differently shaped breakthrough curves (Figure 3-3). The pulse injection leads to a two-tailed breakthrough peak. The maximum normalized concentration (C/C_0) is less than or equal to one. The peak may be skewed, as discussed in Section 2.4.3. The step injection leads to an S-shaped breakthrough curve which reaches $C/C_0=1$ when the column is saturated with tracer.

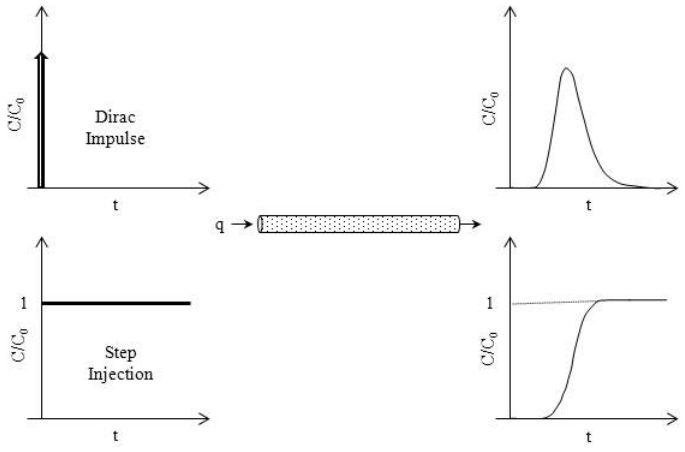

Figure 3-3: Pulse injection (Dirac impulse) vs step injection showing the resulting breakthrough curves. Adapted from Sardin et al., 1991.

For both methods, the moles and mass of tracer injected can be calculated from the ideal gas law. The volume of gas injected for a step injection must be calculated from the flow rate and length of injection, both known. To vary moles of gas injected for a pulse injection, the 100 μL sampling loop can be switched out for a different volume.

3.6 GAS CHROMATOGRAPHY

The downstream end of the column is attached via a 6-port sampling valve with a 100 uL sampling loop to a gas chromatograph with an electron capture detector (SRI Instruments Model 310 GC-ECD), fitted with a heated split/splitless injector. The ECD is very sensitive, allowing for a low concentration of tracer injection as well as lower detection limits. PeakSimple software (version 4.20, SRI Instruments) is used to control the GC and collect data. The carrier gas and makeup gas for the GC-ECD is ultra-high purity nitrogen. Two different columns are used on the GC-ECD, depending on tracer of interest. One measures SF_6 (3' x 1/8'' S.S. molecular sieve 5A packed column [8600-PK3A,SRI Instruments]) and the other measures PFT (15 m x 0.23 mm I.D 10U RT-alumina bond capillary column [19760-280, Restek]). The experimental specifications (column oven temperature, ECD temperature, etc) for individual experiments can be found in Table 3-3.

Table 3-3: Specifications for gas chromatograph for experiments

Injection type	Tracer	Column temp (˚C)	Detector temp (˚C)	Carrier pressure (psi)	Makeup pressure (psi)	Split	Detector current
Pulse	SF_6	40*	150	15	3	Off	240
Pulse	PFT	100	150	15	6	Off	240
Step	PFT	150	100	15	5	On	200

In the case of a pulse injection, the GC is set up to maximize sensitivity. Thus, the detector is at a higher temperature, the detector current is high, and the split is off. This is because the pulse of tracer is diluted significantly during transport through the porous media. Typically, in this scenario, the concentration of the injection is well out of the sensitivity range of the GC. In the case of a step injection, however, the column is fully saturated with tracer and so the GC is configured to minimize sensitivity. To minimize sensitivity, the detector is cooled, the detector current is turned down, and the split is maximized.

3.6.1 Standards

A 102 ppm PMCP in N_2 standard (~2,000 psi) was used for injection on packed columns as well as GC-ECD calibration. The standard was made by Dr. Daniel Riemer of the University of Miami. An SF_6 standard of poorly constrained concentration (~30 ppm) was made and used for injection onto the silica beads and C-soil columns. This standard was made in-house by manually injecting pure SF_6 gas (Sigma Aldrich) into a vessel and pressurizing to a known pressure with pure N_2. Later, a 10.11 ppm SF_6 in N_2

standard (~2,015 psi) was made by Airgas. This SF_6 standard was used for injection on the quartz, illite and B-soil columns as well as GC-ECD calibration.

For GC-ECD calibration, dilutions were made in 1 L Cali-5-Bond™ gas sampling bags fitted with luer-fit valve and Quik-mate connector (GSB-P/1, Calibrated Instruments, Inc). Calibrations were run the day of experiments, just before the experiment began.

3.6.2 Calibration

Calibration of the equipment is essential because the output of the GC must be converted to concentration units to be useful and comparable with other experiments. Although mean residence times and porosity can be estimated without this conversion, normalized concentration values require conversion.

The GC is calibrated using calibration standards, described above. This method uses known concentrations of tracer and correlates these to GC output. Notably, the overall calibration curve for both tracers is nonlinear within the output range of the column experiments, as shown in Figure 3-4.

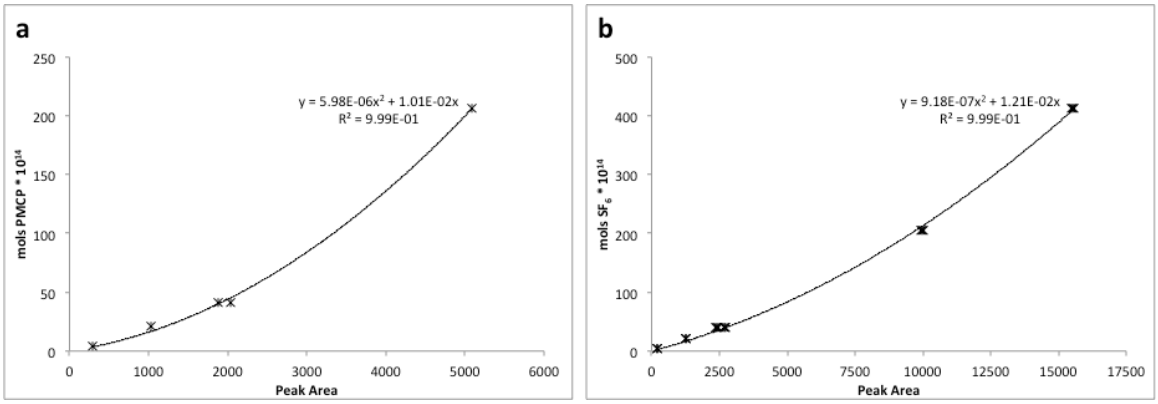

Figure 3-4: Example calibration curves for a) PMCP and b) SF_6

3.7 DATA ANALYSIS

3.7.1 Method of Moments

The method of moments is a commonly used technique to analyze column breakthrough curves. The method of moments may be used to calculate the mean residence times and pore volumes using tracer breakthrough curves. The mean residence time, or first temporal moment, is the single most important property derived from a tracer test (Shook, 2005). The mean residence time is the time weighted average of the tracer history. The following derivation is adapted for 1D, single phase column experiments from Jin et al. (1995) and Shook (2005). For an instantaneous pulse of a single phase, non-reactive tracer in a packed bed, the pore volume can be calculated from the *first moment*, or the mean residence time, $\bar{t}$:

$$\bar{t} = \frac{\int_0^\infty tC_D(t)dt}{\int_0^\infty C_D(t)dt} \quad \textbf{Eq. 3.6}$$

where C_D is normalized tracer concentration:

$$C_D(t) = \frac{C(t) - C_0}{C_{injected} - C_0} \quad \textbf{Eq. 3.7}$$

In the following experiments, C_0 is zero and the integrals are estimated using the trapezoid rule. Each $C(t)$) measurement is run in triplicate at the same time interval.

Levenspiel (1972) shows that the tracer swept pore volume, V_s (the volume of pore space through which the tracer flowed) can be calculated from the mean residence time of a conservative tracer. This is called the *second moment.* In the experiments herein, the tracer is assumed to flow through all of the pore space, or tracer swept pore volume is equal to total pore volume in the column (V_s=V_p).

$$V_P = Q\bar{t}_D \quad \textbf{Eq. 3.8}$$

where Q is volumetric flow [L^3T^{-1}]. Note that V_p includes "dead" volume in the column experimental setup, such as the tubing that connects the autosampler to the column. Therefore, the V_p calculated using the second moment is greater than the actual column pore volume (calculated using known volumes of porous media, see Section 3.4). To accurately know the total pore volume of the column, the dead volume must be independently measured and subtracted from the calculated V_p.

Importantly, the second moment can be used to test whether or not a tracer is conservative in a packing material. If V_p calculated from a breakthrough curve of tracer *i*

is equal to the pore volume of the column calculated from the known volume of porous material, tracer *i* is considered conservative on that column. Here, conservative is defined as a tracer that travels at the mean flow velocity of the carrier gas with no retardation of the tracer by processes such as partitioning or adsorption onto solid materials. However, the density of the packing material must be known for pore volume to be calculated. Density is known for both silica beads and quartz sand columns but poorly constrained for illite and the soils. SF_6 is used to determine pore volume because it is assumed conservative on all columns.

3.7.2 Non-conservative behavior

a. Partition coefficient:

The partition coefficient of tracer *i* between the adsorbed phase and the carrier gas, $K_{a,N}^{i}$, is defined as the ratio of the concentration (mol L^{-3}) of tracer *i* adsorbed onto the porous media (C_{ia}) to the concentration (mol L^{-3}) of tracer *i* in the carrier gas (C_{iN}):

$$K_{a,N}^{i} = \frac{C_{ia}}{C_{iN}} \qquad \textbf{Eq. 3.9}$$

The following relationship, expressed by Jin et al. (1995), is used to find $K_{a,N}^{i}$ using column experiments:

$$K_{a,N}^{2} = \frac{Q}{V_N}(\bar{t}_2 - \bar{t}_1) \qquad \textbf{Eq. 3.10}$$

where $K_{a,N}^{2}$ is the partition coefficient for the reactive tracer between the adsorbed and carrier gas, Q is the volumetric flow rate [$L^3\,t^{-2}$], V_N is the volume of adsorptive material

[L^3], and $\bar{t}_1$ and $\bar{t}_2$ are the mean residence times of the nonreactive tracer and the reactive tracer, respectively. Accurate measurements of the volume or surface area of the adsorptive material (V_N) are often difficult or impossible to obtain. In the following experiments, the volumes of the quartz and silica beads are well known, based on known densities and measured masses that were added. An estimated density of illite of 2.75 g cm^{-3} (Gaines et al., 1997) is applied but the density for the soil remains unknown. An alternative approach is to estimate the volume of material using the method of moments.

b. The Retardation Factor

The retardation factor, R_f, is the ratio of the mean residence time of the reactive tracer, $\bar{t}_2$, and the mean residence time of the non-reactive tracer, $\bar{t}_1$. The retardation factor is the primary variable used to compare the behavior of conservative and non-conservative tracers. It is calculated as:

$$R_f = \frac{\bar{t}_2}{\bar{t}_1} = 1 + \frac{K_{a,N}^2 S_a}{S_N} \qquad \textbf{Eq. 3.11}$$

where S_a is the percent absorbed and S_N is percent in mobile phase (Whitley et al., 1999). The retardation factor is relevant only for a reactive tracer with respect to a nonreactive (conservative) tracer in a particular medium. Therefore, a nonreactive tracer must be identified and used.

c. Statistics

Each tracer experiment is run in triplicate. A two tailed T-test with equal variance is used to test whether or not mean residence times for SF_6 and PMCP in each column are significantly different. The null hypothesis is that the two datasets are the same (i.e. PMCP mean residence times are the same as SF_6 mean residence time and PFT is not retarded). A P-value less than 0.05 rejects the null hypothesis (i.e. PMCP and SF_6 mean residence times are not the same and PFT is retarded). A P-value greater than 0.05 accepts the null hypothesis (i.e. PMCP and SF_6 mean residence times are not significantly different).

3.8 MODELING

The objective of this model is to adequately describe advection-dispersion transport phenomena and to interpret tracer breakthrough curves. Modeling of a 1-dimensional column experiment starts with a partial differential equation that describes non-reactive tracer transport in one-dimension along the x-axis through an isotropic, homogenous porous medium, with constant flow (q) ($\partial q/\partial x = 0$), where q>0 indicates flow in the +x direction. The partial differential equation is based on Fick's second law of diffusion. Advection is accounted for in the diffusion equation by using a moving-coordinates system whereby $x' = x - vt$. The final advection diffusion is:

$$\frac{\partial C}{\partial t} = D^* \frac{\partial^2 C}{\partial x^2} - v \frac{\partial C}{\partial x}, \quad -\infty < x < +\infty \qquad \textbf{Eq. 3.12}$$

where C is concentration [ML^{-3}], D^* is the dispersion coefficient, v is average flow velocity, and x is distance coordinate parallel to flow (Bear, 1979; Fetter, 1999).

3.8.1 Pulse injection of tracer

The solution that describes a column experiment where at t=0 and x=0 a small volume of non-reactive tracer is injected onto the column is derived from Equation 3.12 The following derivation is given by Bear (1979), p. 266.

Initial & boundary conditions:

The concentration of tracer at t=0 is described by the Dirac delta function, $\delta(x)$ (Figure 3-5):

$$C(x,0) = \frac{M}{\phi}\delta(x);\ \delta(x) = \lim_{m\to\infty}\delta_m(x) = \begin{cases}(1/m)\text{for } 0 < x < m, m > 0,\\ 0\ elsewhere\end{cases}$$

$$M = \int_{-\infty}^{+\infty} nC(x',t)dx'$$

where $x' = x - vt$, M is mass (M), ϕ is porosity and C is concentration (M L^{-3}). Thus, at t=0, concentration of tracer is 0 everywhere except at x=0 where a small finite volume of tracer exists. The boundary condition of *x'* is:

$$\lim C(x',t) = 0, \quad |x'| \to \infty$$

which means that concentration of tracer approaches 0 as distance increases to infinity.

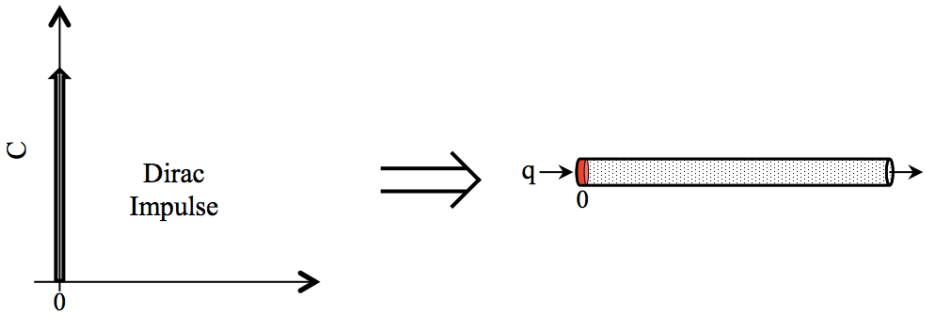

Figure 3-5: Illustration of the Dirac delta function a) graphically and b) on the column at t=0. A small volume of tracer (red) is injected onto the upstream end of a packed column.

Solution: Using these initial and boundary conditions, the analytical solution to this model is

$$C(x,t) = \frac{M}{A\phi R\sqrt{4\pi \mathrm{D}t/R}} \exp\left(-\frac{x-(vt/R)^2}{4Dt/R}\right) \qquad \textbf{Eq. 3.13}$$

where A is area (L^2), ϕ is porosity, R is a retardation factor, D is hydrodynamic dispersion (L^2 t^{-1}), t is time, and v is average linear velocity (L t^{-1}). Equation 3.13 is programed into Matlab (2010) to model the SF_6 breakthrough curves. The model uses a least squares regression to best-fit experimental data with the coupled advection-dispersion equation.

The parameters allowed to best-fit are flow velocity, hydrodynamic dispersion and mass injected. For hydrodynamic dispersion, the starting value is the binary diffusion coefficient. In the case of SF_6 and N_2, the binary diffusion coefficient was calculated using the Fuller Equation (Section 2.4.2). The diffusion volumes for N_2 and SF_6 are 17.9 and 69.7, respectively (Fuller et al., 1966). The binary diffusion coefficient is determined

to be 0.0985 $cm^2\ sec^{-1}$. The diffusion volume for PMCP is not known and published information on the diffusion coefficient between PMCP and N_2 is not available. The starting value used is the binary diffusion coefficient for PMCH into air, 0.05 $cm^2\ sec^{-1}$ (Sullivan et al., 1996).

3.8.2 Peak Tailing

One important quality of this model, in contrast to the very simplistic models of advection-diffusion described in Section 3, is that this equation predicts asymmetry (i.e. tailing) in the breakthrough curves. Tailing is a ubiquitous characteristic of tracer breakthrough curves in real geologic media (e.g. Jackson et al., 1984; Jin et al., 1995; Nelson et al., 1999). Understanding the causes and controls of tailing is useful to interpreting column breakthrough curve experiments. Tailing is caused by fundamental properties of the porous medium as well as the interaction of a sorbing gas with the porous medium. The physical causes of asymmetric peaks are discussed in Section 2.5.4. Figure 3-6 illustrates how several important variables in the advection-dispersion equation affect peak tailing.

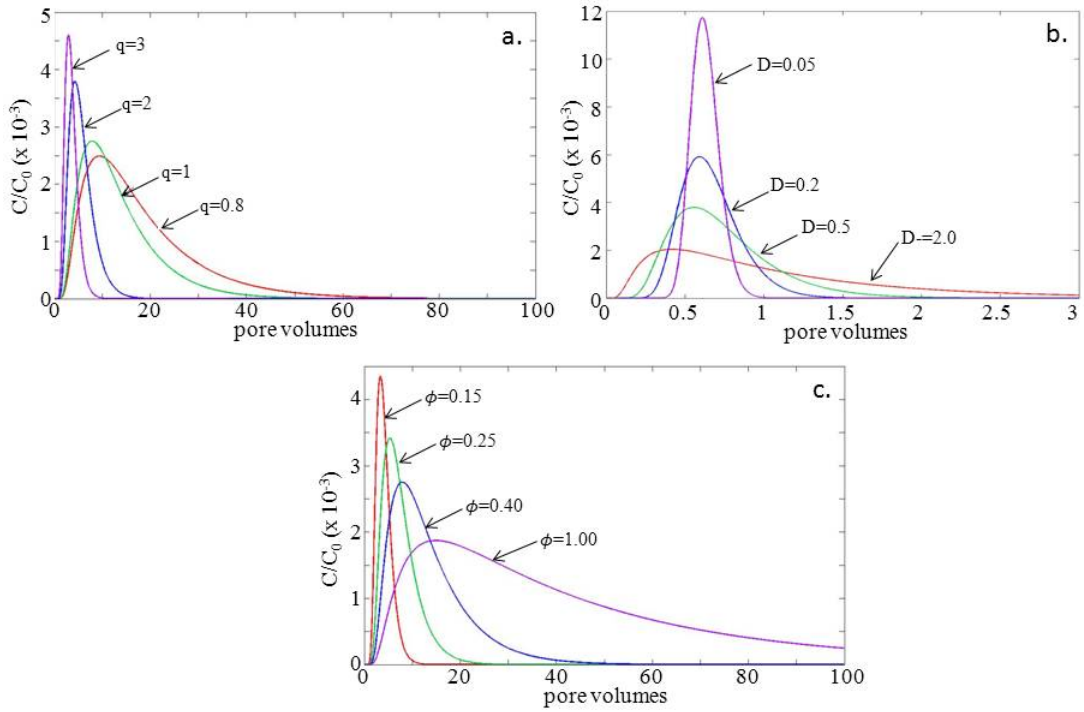

Figure 3-6: Illustration of peak tailing due to changes in model parameters: a) volumetric flow rate, b) hydrodynamic dispersion coefficient and c) porosity.

Long tails are caused by: decreasing the flow rate, decreasing the porosity, and increasing the hydrodynamic dispersion term. These factors are not independent; decreasing the porosity increases tortuosity and thus the hydrodynamic dispersion coefficient.

4. Results

This section reports the result from media analyses and column experiments. The results are in the form of 1) tables and figures to summarize the results of media analyses, 2) tables to summarize experimental data such as flow rates, average velocities, mean residence times, and estimated Péclet numbers, and 3) figures showing tracer response curves for both SF_6 and PMCP on each column.

The mean residence times are provided in each figure. The x-axis is in mL eluted, which is simply the time multiplied by the flow rate. All experiments are run in triplicate. In all but two cases (PMCP on B-soil and illite), breakthrough curves are shown as an average because the curves replicated very well. Error bars show the range. In some cases the range is too small to be visible on the plotted data. In the case of PMCP breakthrough on B-soil and illite, all three curves are shown because they do not replicate well.

4.1 Media Analysis

4.1.1 Particle Size Distribution and Surface Area

The quartz sand and silica beads have approximately the same average particle size but the quartz sand has a wider particle size distribution. The soil and illite aggregates both have a larger average particle size and larger particle size distribution than the quartz sand and silica beads. Illite is in aggregate form.

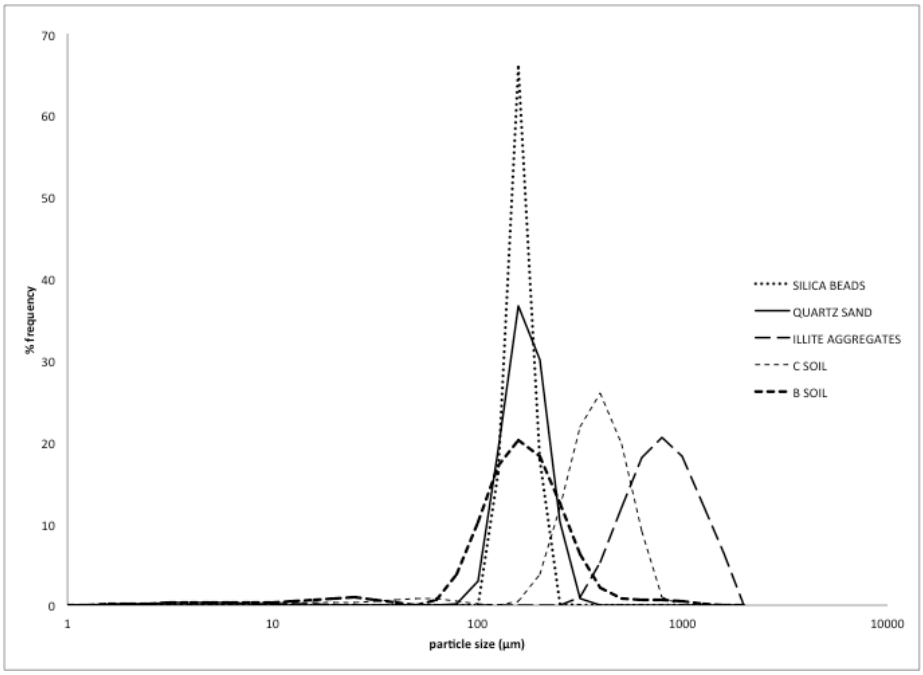

Figure 4-1: Particle size distribution for the 5 packing materials used in the following experiments.

Table 4-1: Summary of size distribution of packing materials. D50 is the median grain size; 10% of particles are smaller than the D10 grain size; 90% of particles are smaller than the D90 grain size.

	Packing material	**Sieve size (US sieve)**	**D10 µm**	**D50 µm**	**D90 µm**
A	Acid-washed slilca beads	0.211-0.152 (70-100)	152 ± 0	178 ± 0	207 ± 0
B	Quartz sand	0.251-0.125 (60-120)	142 ± 0	190 ± 1	255 ± 0
C	Illite	Not sieved	519 ± 17	902 ± 27	1590 ± 72
D	C-soil (organic-rich)	0.422-0.125 (40-120)	247 ± 4	419 ± 2	632 ± 2
E	B-soil (organic-poor)	Not sieved	98 ± 0	182 ± 0	327 ± 3

Surface area results from BET analyses (Table 5-2) show very high specific surface area for illite (1.84×10^5 cm^2 g^{-1}), an order of magnitude higher than that of C-soil (8.50×10^4 cm^2 g^{-1}). Illite also has the highest total surface area in the columns (2.21×10^6 cm^2). The lowest specific surface area is that calculated for the B-soil assuming perfect sphere geometry (1.25×10^2 cm^2 g^{-1}), although this calculation is an underestimate due to the irregular grain size of the media.

Table 4-2: Surface area of packing materials. Note that a star (*) indicates measurements taken by BET analyzer (illite aggregates and C-soil). Otherwise, figures are calculated using particle size distribution data, assuming perfect sphere geometry.

Packing Material	**Specific surface area cm^2g^{-1}**	**Total surface area in column cm^2**
Silica beads	1.43×10^2	1.84×10^4
Quartz sand	1.33×10^2	1.71×10^4
*Illite aggregate	1.84×10^5	2.21×10^6
*C-soil	8.50×10^4	3.00×10^4
B-soil	1.25×10^2	1.99×10^3

4.1.2 Mineralogy and Organic Carbon

The B-soil was found to have 0.4 ± 0.02 wt% organics. The C-soil was found to have 38 ± 1 wt% organics. The XRD results indicate that B-soil is high SiO_2 and without other significant mineral signatures. The C-soil did not match most known soil mineral constituents except silica. The high organic content may have complicated the analysis

4.2 COLUMN EXPERIMENT SUMMARY

PMCP is retarded with respect to SF_6 in all five columns tested. Retardation factors range from 1.1-139. The largest retardation factor occurs on illite aggregates. A summary of these results is presented in the tables, below. The partition coefficient, $K_{a,N}^2$, for illite is calculated using a PMCP mean residence time of 501.8 minutes. The partition coefficient for B-soil is calculated using a mean residence time for PMCP of 28.4 minutes.

Table 4-3: Summary of results from pulse injections of SF_6 and PMCP onto five packed columns.

	$\bar{t}_{SF6}$	$\bar{t}_{PMCP}$	R_f	$K_{a,N}^2$
	min	**min**	**--**	
Silica beads	30.9	34.2	1.1	0.09
Quartz sand	20.7	22.9	1.1	0.10
Illite	5.0	501.8 - 701.4	100 - 139	107.17
C-Soil	32.6	76.6	2.3	1.37
B-Soil	28.4	625.0	19.4-20.9	49.21

Note that the illite PMCP mean residence times have a range due to poor reproducibility of PMCP breakthrough curves. Also note that all experiments are run in triplicate.

Table 4-4: Comparison of pore volumes (mL) and porosity predicted using the SF_6 breakthrough curve (method of moments) and the measured values.

	Method of Moments		**Measured Values**	
	Pore Vol	ϕ	**Pore Vol**	ϕ
Silica Beads	38.6	0.47	33.2	0.41
Quartz Sand	10.4	0.63	5.4	0.33
Illite	5.0	0.60	4.0	0.48
C-soil	32.6	0.69	15.1	0.32
B-Soil	14.2	1.42	4.0	0.39

Table 4-4 shows the comparison of the pore volume and porosities measured from the method of moments using the SF_6 breakthrough curve and the measured values. Note the discrepancy between method of moments calculations and measured values.

4.3 SILICA BEADS

Figure 4-2 shows the breakthrough curves of pulse injections of SF_6 and PMCP on a column packed with acid washed silica bead. The flow rate for this experiment is 1.25 mL min^{-1} for both tracers. The average velocity is 0.0136 cm s^{-1}. PMCP is retarded with respect to SF_6 ($p>0.05$). The average mean residence time for SF_6 is 30.9 minutes whereas the average mean residence time for PMCP is 34.2 minutes. The retardation factor is 1.1. To test whether or not SF_6 behaves conservatively, we compare the measured porosity with the porosity calculated from $\bar{t}_{SF6}$ using Equation 3.8. The measured porosity is 40.6% (including 2.5 mL dead volume) and the porosity calculated from the second moment of the SF_6 breakthrough curve is 47.5%. This corresponds to a measured pore volume of 33.2 mL and a pore volume calculated from the second moment of 38.6 mL.

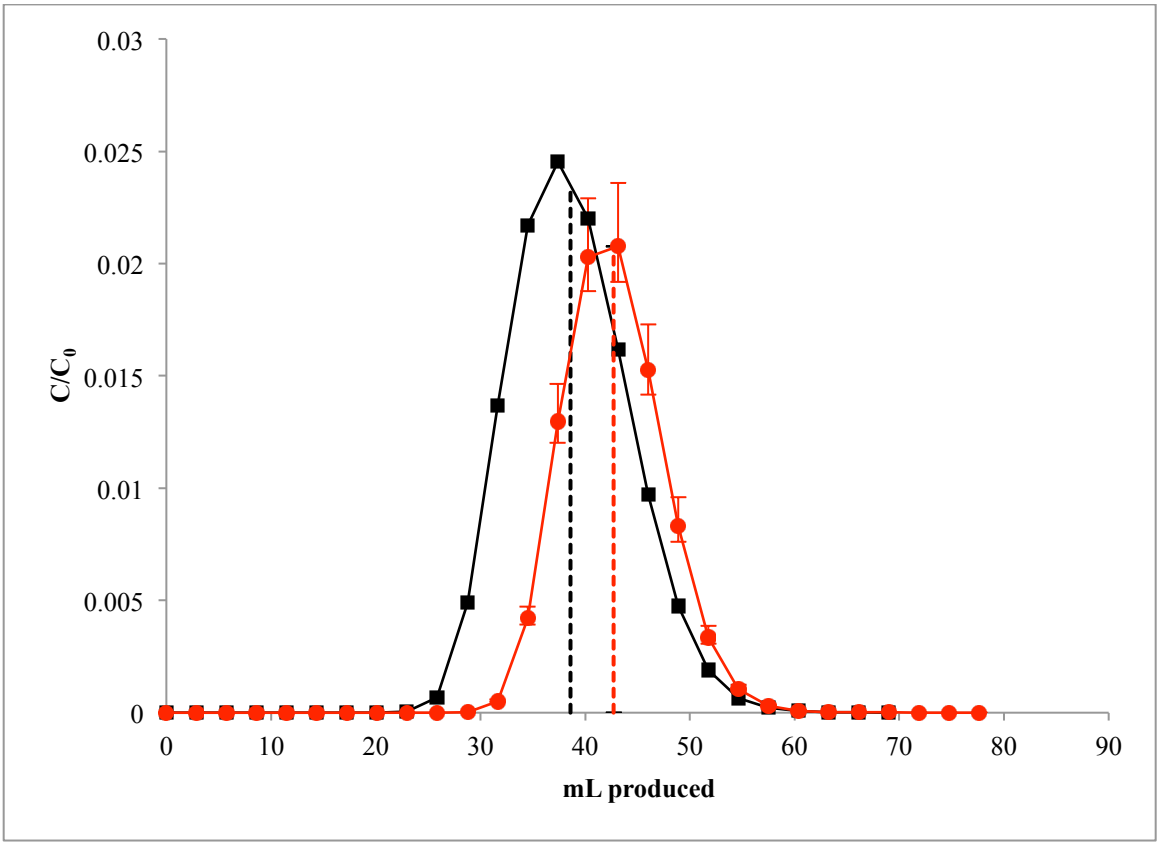

Figure 4-2: Breakthrough curves for pulse injections of SF_6 (black squares) and PMCP (red circles) through column packed with acid washed silica beads. The mean residence time for PMCP (dotted red line), $\bar{t}_{PMCP}$, is 34.2 min. The mean residence time for SF_6 (dotted black line), $\bar{t}_{SF6}$, is 30.9 min. The retardation factor, R_f, is 1.1.

4.4 Quartz Sand

Figure 4-3 shows the breakthrough curves of pulse injections of SF_6 and PMCP on a column packed with quartz sand. The flow rate for this experiment is 0.5 mL min^{-1} for both tracers. The flow rate is slower because the pore volume is much smaller (the slower flow rate allows for better capture of the peak shape). The average velocity is 0.02 cm s^{-1}. PMCP is retarded with respect to SF_6 ($p>0.05$). The mean residence time for

SF_6 is 20.7 minutes whereas the breakthrough time for PMCP is 22.9 minutes. The retardation factor is 1.1. The measured porosity is 32.7% (including 2.5 mL dead volume) and the porosity calculated from the second moment of the SF_6 breakthrough curve is 63.1%. This corresponds to a measured pore volume of 5.4 mL and a pore volume calculated from the second moment of 10.4 mL. Note the skewness of the curves; the breakthrough curves on quartz sand are more skewed than those on silica beads due to increased tortuosity.

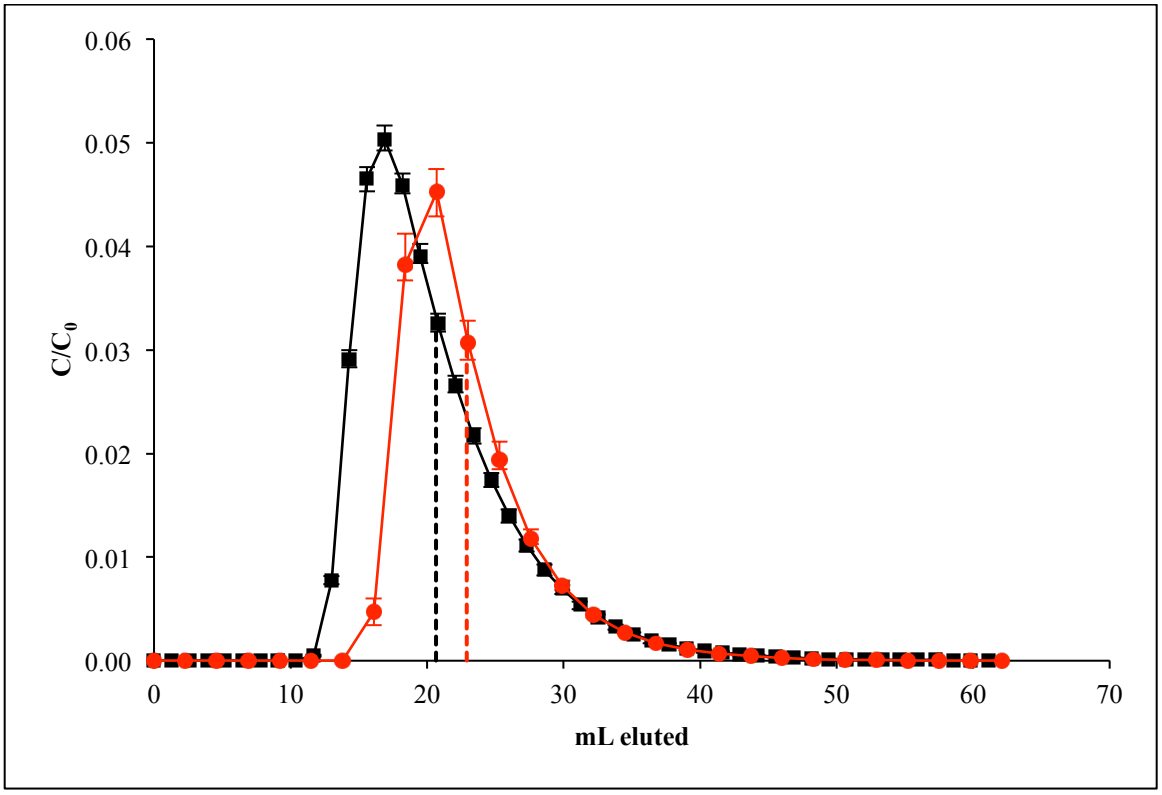

Figure 4-3: Breakthrough curves for pulse injections of SF_6 (black squares) and PMCP (red circles) through column packed with quartz sand. The mean residence time for PMCP (dotted red line), $\bar{t}_{PMCP}$, is 22.9 min. The mean residence time for SF_6 (dotted black line), $\bar{t}_{SF6}$, is 20.7 min. The retardation factor, R_f, is 1.1.

4.5 ILLITE

Figure 4-5 shows the breakthrough curves of pulse injections of SF_6 and PMCP on a column packed with illite. Note the x-axis is in log scale. The flow rate for PMCP experiments is 4 mL min^{-1}. The flow rate for the SF_6 experiments is 1 mL min^{-1}. The flow rate was increased for PMCP compared to SF_6 because of the very slow elution of PMCP from the column; the slower flow rate leads to long experimental time as well as dilution of PMCP. PMCP shows poor reproducibility.

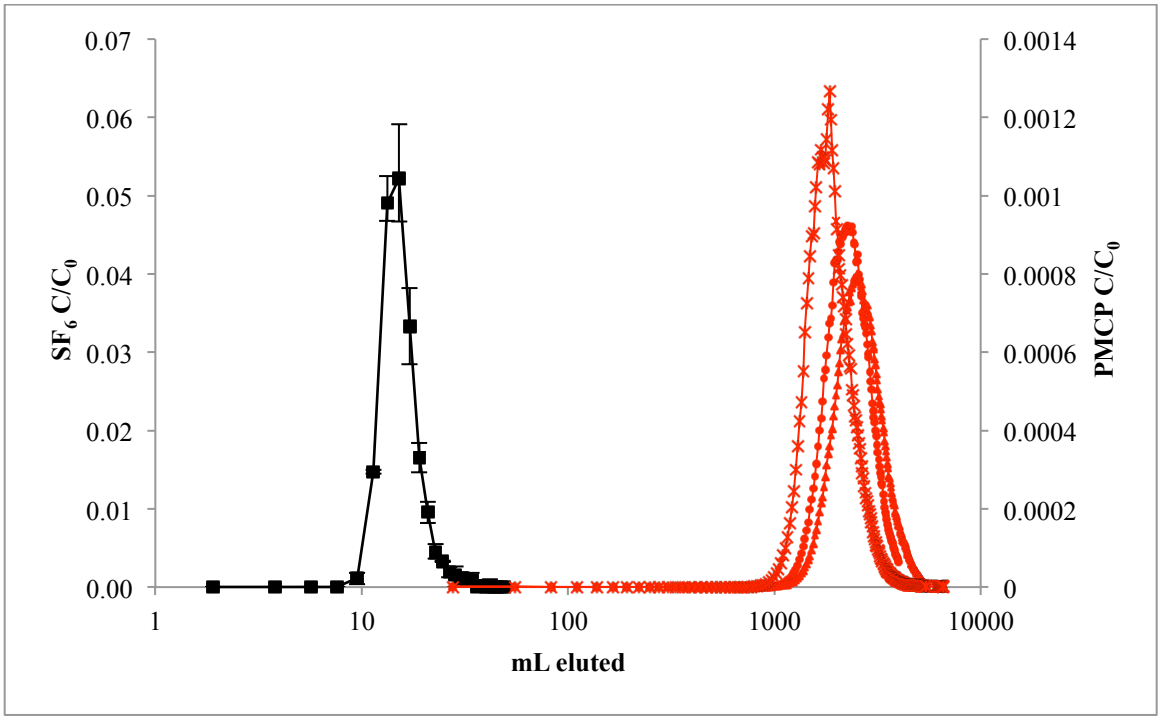

Figure 4-5: Breakthrough curves for pulse injections of SF_6 (black squares) and PMCP (1st injection= red circles, 2nd injection= red triangles, 3rd injection=red stars) through column packed with illite aggregates. X-axis is log scale.

The average velocities are 0.478 and 0.120 cm s^{-1} for PMCP and SF_6, respectively. The mean residence times for the three injections of PMCP, $\bar{t}_{PMCP}$, are

528.5 min, 701.4 min and 501.8 min, respectively. The mean residence time for SF6, $\bar{t}_{SF6}$, is 5.0 min. The retardation factors, R_f, are 105, 139, and 100, for replicates 1 - 3. The measured porosity is 47.7% (including 2.5 mL dead volume) and the porosity calculated from the second moment of the SF_6 breakthrough curve is 59.7%. This corresponds to a measured pore volume of 4.0 mL and a pore volume calculated from the second moment of 5.0 mL.

4.6 C SOIL

Figure 4-6 shows the breakthrough curves of pulse injections of SF_6 and PMCP on a column packed with C-soil. The flow rate for this experiment is 1.00 mL min^{-1} for both tracers. PMCP is retarded with respect to SF_6. PMCP is retarded with respect to SF_6 ($p>0.05$). The mean residence time for SF_6 is 32.6 minutes whereas the breakthrough time for PMCP is 76.6 minutes. The retardation factor is 2.3. Note the long tail on the PMCP breakthrough curve compared to the short tail on the SF_6 breakthrough curve.

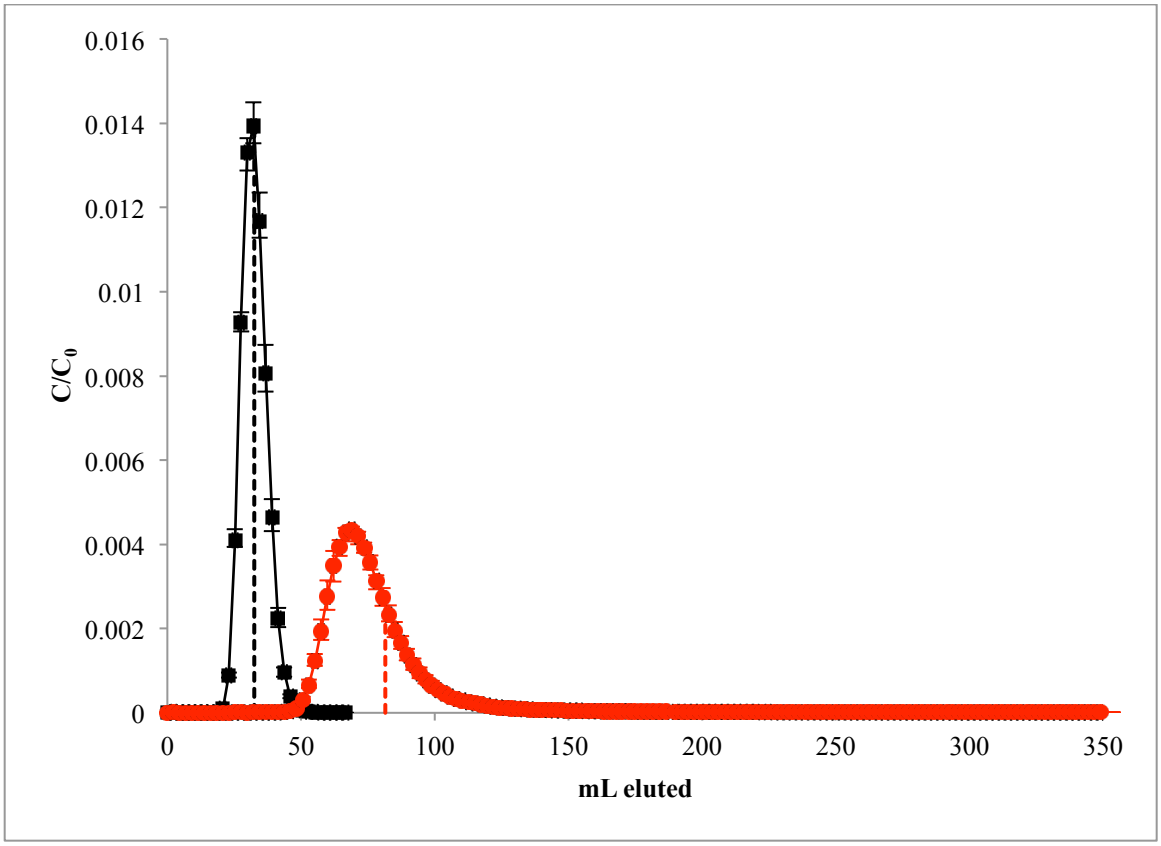

Figure 4-6: Breakthrough curves for pulse injections of SF_6 (black squares) and PMCP (red circles) through column packed with C-soil. The mean residence time for PMCP (red dotted line), $\bar{t}_{PMCP}$, is 76.6 min. The mean residence time for SF_6 (black dotted line), $\bar{t}_{SF6}$, is 32.6 min. The retardation factor, R_f, is 2.3.

The second experiment on the B-soil was a step-injection used to determine the adsorption isotherm for PMCP. A comparison of the breakthrough curve with Figures 1 and 3 in Buergisser et al. (1993) is shown in Figure 4-7. The purpose of this experiment is to qualitatively test whether PMCP follows a linear, concave or convex adsorption isotherm on the C-soil using the method presented in Buergisser et al. (1993) (Section 2.4.5.)

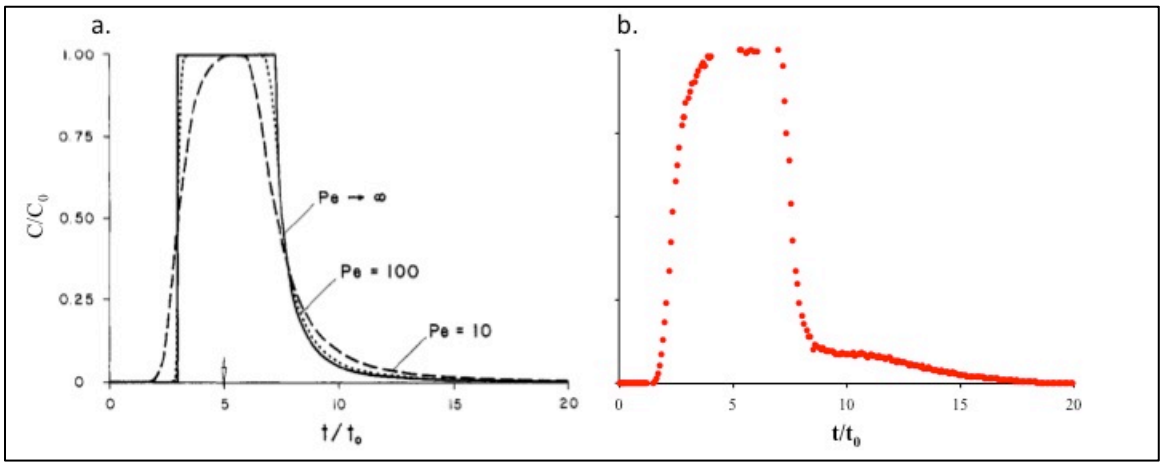

Figure 4-7: Comparison of the case of a convex Freundlich isotherm from Buergisser et al. (1993) (a) with the breakthrough curve for step injections of PMCP through column packed with C-soil (b). The Péclet numbers indicated are calculated as vL/D_L. The Péclet number for the experimental data is 22.

Results show that experimental data follow a convex isotherm from $0<t/t_0<9$. At about $t/t_0=9$, on the desorption branch, the relative concentration changes slope abruptly. This suggests a more complex desorption mechanism is contributing to the release of PMCP, possibly due to small aggregates existing in the C-soil where diffusive transport is occurring or kinetically-moderated desorption that leads to a slow release of compound. These more complicated processes would be expected for a natural soil as well as clay minerals like illite. The Péclet number for the experiment, calculated as vL/D_L, is 22. This compares favorably with the convex isotherm with $10<Pe<100$.

4.8 B SOIL

Figure 4-8 shows the breakthrough curves of pulse injections of SF_6 and PMCP on a column packed with B-soil. The flow rate for this experiment is 0.5 mL min^{-1} for

both tracers. PMCP is retarded with respect to SF_6. The PMCP curves do not reproduce well. The mean residence time for SF_6 is 28.4 minutes whereas the mean residence times for PMCP are 595.34 min, 554.84 min and 551.32 min. The retardation factors are 20.9, 19.5 and 19.4, respectively

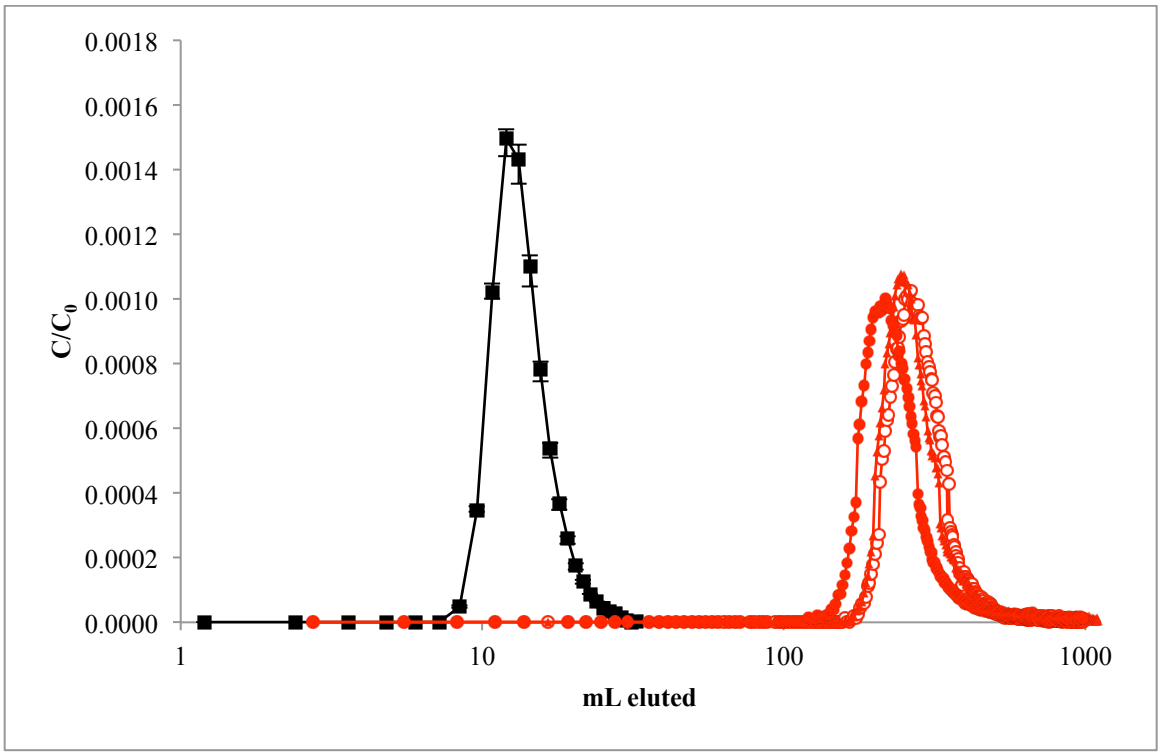

Figure 4-8: Breakthrough curves in B-soil for pulse injections of SF_6 (black squares) and PMCP (1st injection= empty circles, 2nd injection= red triangles, 3rd injection=red circles). The mean residence times for PMCP are 595.34 min, 554.84 min and 551.32 min. The mean residence time for SF6, $\bar{t}_{SF6}$, is 28.4 min. The retardation factors, R_f, are 20.9, 19.5 and 19.4..

4.9 MODELING

Figure 4-9 shows the model fitted to the laboratory breakthrough curve for SF_6 in silica beads. The model has 7 variables: flow velocity, dispersion, retardation factor,

mass injected, porosity, column length and area. Of these 7 variables, 4 are well constrained: porosity, column length, area, and retardation factor. Porosity is 0.41, column length is 99.822 cm, area is 0.1640 cm^2, and the retardation factor is 1 (no retardation).

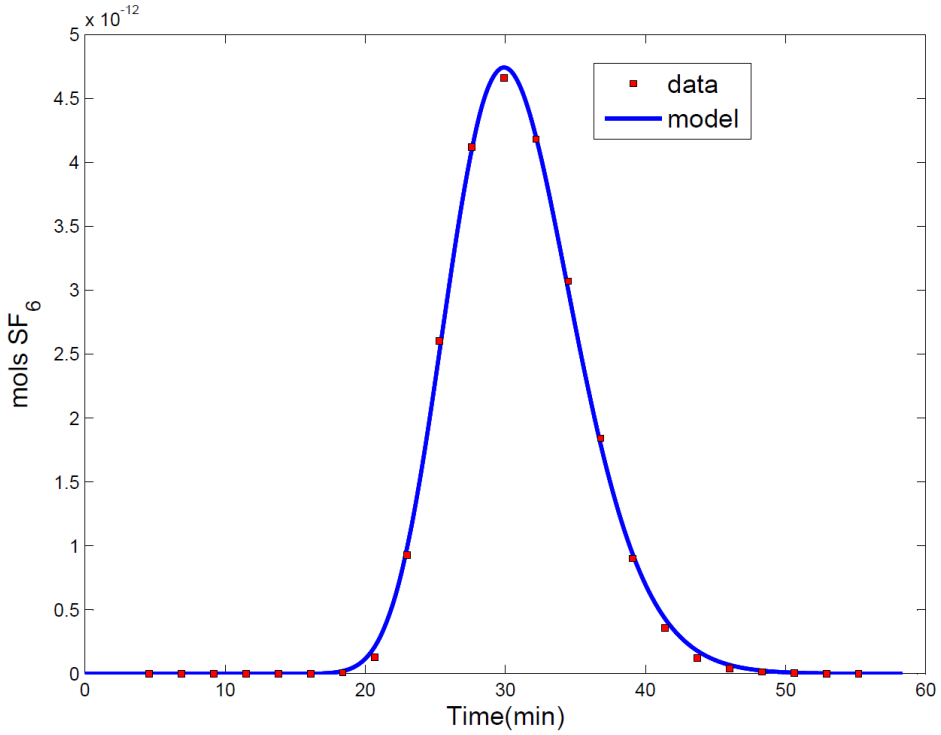

Figure 4-9: Model of SF_6 breakthrough on silica beads column

The other 3 variables (flow velocity, dispersion and mass injected) were best fit using a least squares regression. The above fit yielded a flow velocity of 0.0550 cm s^{-1}, a dispersion of 0.0609 cm^2 s^{-1}, and a mass injected of 1.1851 x 10^{-11} kg. The model flow velocity is slower than that calculated from the flow controller and the porosity (0.062 cm s^{-1}), an 11% difference. The hydrodynamic dispersion is lower than pure diffusion

predicted from the Fuller equation (0.0985 cm^2 s^{-1}). This is unexpected because the hydrodynamic dispersion is affected by tortuosity and mechanical dispersion and should be higher than diffusion. Notably, the mass injected for this experiment is poorly constrained. This is because the standard injected was made in-house rather than by the AirGas standard and the actual concentration is not known, so it is difficult to attribute possible error estimates. The mass does not affect peak width, tail shape or mean residence time but it does affect peak height. The peak height is very sensitive to this term.

5. Discussion

This section contains a discussion of 1) the potential mechanisms for PMCP retardation and peak shape for each column, 2) the limitations of this work and recommendations for further research, and 3) the implications of this work for CCS monitoring and verification.

5.1 PMCP Retardation

The hypothesis that PMCP would behave conservatively (R_f=1) on silica beads and quartz sand but non-conservative on illite and natural soils is proven false. PMCP was retarded with respect to SF_6 (R_f>1) in all experimental simulations, including in columns packed with silica beads and quartz sand. PMCP had the highest retardation factor on illite column.

Possible mechanisms of non-conservative behavior include: 1) partitioning into soil organic matter, 2) adsorption onto mineral surfaces, and 3) condensation into the liquid phase. Partitioning into water or adsorption at the gas-liquid interface will not be considered as these are dry experiments.

5.1.1 Silica Beads and Quartz Sand

a. The Mechanism of Retardation of PMCP

Two potential mechanisms may cause retardation of PMCP on the quartz sand and silica beads: physisorption due to van der Waals force and condensation of PMCP in cool spots along the column. The latter is likely the more important of the two: the boiling point of PMCP at atmospheric pressure is 48.1 °C. The column was wrapped in heat tape at ~60 °C and the GC oven is heated to 100 °C, so condensation to liquid is not expected to occur in these areas. However, the connecting tubing from the PMCP tank to the column and from the column to the GC were at room temperature (~26 °C) and condensation may have occurred in these areas, which may have contributed to retardation of PMCP with respect to SF_6. This results in non-conservative behavior (R_f>1), even in the absence of sorption or partitioning.

Physisorption, though it may occur, does not appear to be the driving force behind retardation of PMCP in these columns filled with silica bead and quartz sand. Silica beads and quartz sand have the same mineralogy but differ in their surface area and grain size distribution. Quartz sand has a higher surface area due to its irregular shape and rough surface. If van der Waals forces were the cause of retardation, one would expect larger retardation on the column with larger surface area. However, both column experiments result in the same R_f (1.1). Assuming the difference in surface area between

the two media is sufficient to produce different R_f values, this result indicates that van der Waals are not the mechanism of retardation in this material.

Finding and correcting the cold spots in the experimental setup would test this conclusion. If cold spots cause retardation of PMCP, one would expect the retardation to decreases or be eliminated with a better column setup. This result highlights the importance of good experimental setup for column experiments. It also highlights the issue of PFT condensation in a field setting, where temperatures may fall below the boiling point along a leakage pathway from the injection zone to the NSMZ. This would result in non-conservative behavior even in the absence of chemio- or physiosorption, a major challenge for quantifying CO_2 leakage rates.

b. Peak Tailing and Curve Shape

There are marked differences in the shapes of the breakthrough curves in these materials. As discussed in Section 2.4.3, peak tailing may be caused by slower flow rates, lower porosity, and higher hydrodynamic dispersion due to increases in, for example, tortuosity. Quartz sand experiments have a slower flow rate than silica beads experiments (0.50 mL min^{-1} vs. 1.25 mL min^{-1}), a lower porosity (0.33 vs. 0.41), and higher hydrodynamic dispersion due to increased tortuosity. The latter is inferred and cannot be well constrained due to limited knowledge of the tortuosity coefficient, ω. These observations highlight the importance of understanding the properties of the

porous medium as well as constraining the experimental parameters in order to correctly interpret and predict breakthrough curves, both in laboratory settings and in the field.

5.1.2 Illite

On the illite column, PMCP has an average retardation factor ranging from 100-139 with respect to SF_6. The retardation of PMCP onto illite is most likely due to physisorption of PMCP via electrostatic attraction between the surface of the clay and the PMCP molecules as well as contributions from phase partitioning as described earlier. This electrostatic reaction of physiosorption occurs because PMCP has a high electron affinity due to its structure and large number of fluorine atoms and the illite has unbalanced negative charges at the surface (Cooke et al., 2001). The sorption process in illite is enhanced by the media's very high specific surface area (1.84×10^5 cm^2 g^{-1}) and micropore structures, lending many adsorption surfaces.

5.1.3 C-Soil

In the C-soil, PMCP is retarded with respect to SF_6 by a factor of 2.5. The C-soil has a high organic content and low clay content and the retardation of PMCP is most likely due to sorption of PMCP onto the soil organic matter. Soil organic matter is a well-documented sorptive material in the vadose zone (e.g. Pennell et al., 1992). Because soil organic matter is common in the vadose zone, particularly near ground surface, characterizing soil organic carbon content before choosing tracers will be important.

5.1.4 B-Soil

The B-soil experiments yield higher retardation of PMCP than the C-soil experiments, despite lower organic carbon content (<1%). Therefore, though organic carbon content may contribute to PMCP retardation in the B-soil, there is likely an additional constituent causing retardation. This additional material may be clay. The illite column experiments yielded high retardation of PFTs (R_f>100), showing that PMCP may have much higher sorption onto illite than an equivalent mass of soil organic matter. Sorption of nonpolar organic vapors onto anhydrous soil materials has been shown to be primarily the result of adsorption on internal surfaces rather than uptake by soil organic matter (Pennell et al., 1992), particularly in low to no water vapor environments (Breus and Mishchenko, 2006). This evidence supports the possibility that PMCP sorption is much stronger on clays than organic matter content.

However, the clay content in the B-soil is not well constrained. The particle size distribution is not a perfect method to determine total clay content because the soil was not disaggregated before particle size analysis. Clays may be in aggregate or colloidal form. Additionally, the XRD analysis showed the B-soil to be well-matched, but not perfectly matched, to silica but did not determine other mineral constituents. Thus, the B-soil may contain a higher portion of clay than is clear from its particle size distribution or XRD. Clay content in the B-soil is a possible cause of retardation on this column.

5.1.5 Poor Reproducibility

PMCP breakthrough curves have poor reproducibility on the illite and B-soil columns (in which retardation is large), whereas the SF_6 breakthrough curves reproduce very well. Several possible causes for this include a) the slow release of water from the interstices of clay minerals, b) variation in the mass of tracer injected, and c) poor flow control by the flow controller.

If slow release of water from the clay minerals causes an increase in sorption sites, one would expect increased retardation and peak tailing with each successive experiment due to increase in adsorption sites. However, on illite, the successive peak breakthrough, mean residence time and shape do not follow a clear pattern; the shortest breakthrough occurs on the third experiment and the longest occurs on the second. The third breakthrough curve also appears to have irregular ECD response near the peak of the curve. These results suggest that slow release of water and increase in sorption sites is not a primary cause of variability.

Alternatively, if removal of water from clay interstices causes clay structures to change, such a pattern would not be expected. Clays have been shown shrink or crack due to desiccation (Albrecht and Benson, 2001; Augier, 2002). These structural changes lead to changes in hydraulic properties of the clay (Day, 1997; Boynton and Daniel, 2008), which would likely cause changes in retention time and potentially peak shape of tracer breakthrough curves.

Regarding the variation of injection mass, Buergisser et al. (1993) show that peak breakthrough and residence time depend on amount of tracer injected. Slight changes in amount of time the auto-injection loop is allowed to flush, temperature and pressure may potentially cause changes in the amount of tracer injected. Also, the illite column injection volume is higher than for other experiments (500 μL), and this larger injection loop could cause greater variability in injected mass.

The variability in injection mass would be common across all experiments, but is manifested more clearly in experiments which last 19 hours or more. PMCP has a slower average velocity than SF_6 (due to sorption), so the distance between the tracer masses increases with time. This difference may be too small to detect for short experimental times but, because it increases with increasing experimental time, detectable for the illite and C-soil experiments. Given this evidence, changes in the mass of the injected tracer coupled with the length of the experiment and potentially clay desiccation are the most likely causes for poor reproducibility of PMCP breakthrough curves on illite and B-soil columns.

5.1.6 SF_6 behavior

In our experiments, we assume SF_6 is conservative for the purpose of comparison with PMCP. This is a reasonable assumption based on past research (e.g. Olschewski et al., 1995; Wilson and Mackay, 1996; Mariner et al., 1999). However, SF_6 does not meet the stated criterion for conservative behavior in the present experiments because the

second moment of the SF_6 breakthrough curve overestimates the measured pore volume. Though this discrepancy does not present a problem for the purpose of evaluating PFT retardation, insight was gained from analyzing the potential causes of the discrepancy. Even correcting for dead volume (~2.3 mL), the second moment for the SF_6 breakthrough curve on silica beads yields a pore volume of 39 mL and the measured pore volume is 33 mL. In the case of quartz sand, the second moment yields a pore volume of 10.3 mL, while the measured pore volume is 5.1 mL. The same pattern is true for illite and both soil columns, though the density of these materials is not well constrained and so this discussion will be limited to quartz sand and silica beads.

There are several possible causes for this discrepancy, discussed above: a) poor flow control, b) poor constraint on dead volume, and c) immobile spaces in the porous media. The possibility of poor flow control is discussed above (Section 5.1.5) and may be solved by adding a flow meter at the outlet of the column to ensure that the flow controller is accurate. Regarding the dead space, the second moment calculation includes both the pore space in the porous media as well as in the experimental setup, or the dead space. The experimental setup for each experiment changed slightly between experiments (length of tubing, size of connections) and this change is not considered in the dead volume included in my calculations. This may change the dead volume by several mL, which would make the second moment calculation inaccurate.

The third possibility is immobile regions in the pore network. In other words, dead-end pores or micropores may exist within the pore network which cause temporary stagnation of tracer. Mobile-immobile type transport is common in porous media exhibit multiple pore domains due to layering, fracturing or aggregation (Leij et al., 2012). Mobile-immobile flow has been well researched, documented and modeled (e.g. De Smedt and Wierenga, 1979; Šimůnek et al., 2003). This type of pore network is not expected in the case of silica beads, which are perfect spheres, but may occur in the other porous media.

This type of transport would lead two different flow regimes in the porous media: advection-dominated transport in larger pores and diffusion-dominated in smaller pores (De Smedt and Wierenga, 1979). The resulting breakthrough curve would have an elongated tail (De Smedt and Wierenga, 1979; Sardin et al., 1991; Leij et al., 2012), which would cause non conservative behavior even in the absence of sorption, partitioning or phase change. Thus, the second moment would overestimate the actual pore volume.

5.1.8 Modeling

The modeling succeeds in fitting the experimental data to a basic advection-dispersion equation, thus demonstrating that experimental conditions were consistent with the model setup and the potential for more predictive tracer experiments. The model results serve several other purposes, including understanding the sensitivities and

limitations of the present experimental data, demonstrating fundamental understanding of advection and dispersion, and establishing a modeling platform to aid in future laboratory and field experiments.

Regarding the first purpose, the model elucidates a key limitation of these experiments. Namely, poor control of injected tracer mass as well as poorly constrained GC calibration. The ramifications of this are that 1) tracer mass recovery (amounted of tracer recovered vs. amount of tracer injected) is not known with certainty and 2) interpretation of the model results is limited because mass injected is best-fit rather than defined. Understanding tracer mass recovery is important to confirm that the tracer is not sorbed onto or reacted with the fluid or porous media in the column and the column is air-tight. In these experiments, yield is assumed to be 1 (i.e., all tracer is recovered) because the tracer is allowed to elute until background is below detectable limits and the column is leak tested. However, these precautions are not perfect proof, so yield = 1 cannot be verified without better control on injection volume and GC calibration.

5.2 Limitations and Recommendations

These experiments provide important preliminary information to evaluate the behavior of PFTs in the vadose zone. They also provide a platform from which to evaluate a number of different tracers on a porous media of interest as well as a simple model and data analysis scheme to interpret the data. Several experimental issues were encountered and identified that will aid future researchers in designing more rigorous column experiments. As such, these results are limited and several important aspects of tracer transport were not considered. Here, I describe two key limitations of these

experiments that affect the interpretation of these data and their relevance to natural systems.

5.2.1 Material choice, affinity and surface area

These column experiments test only for the presence of retardation due to adsorption and they do not provide more detailed insight into the specific process of adsorption. If the goal of the tracer column experiment is to determine whether adsorption occurs on a particular vadose zone material for a tracer, this information is sufficient. However, for better understanding of the adsorption processes and potential implications for vadose zone monitoring programs, further testing is required.

To generalize the findings of this study, PFT retardation should be tested on more end-member type porous media. In this study, PFT retardation was tested on pure quartz and pure illite. Results from these experiments thus relate only to substrate with quartz or illite. In contrast, rather than test end-member type organic materials (e.g. pure cellulose or leaf matter) this study uses two soils with complex and uncharacterized soil organics. Results from these experiments relate to the vadose zone where the materials were sourced but indirectly to other vadose zones with organic material.

Additionally, this study does not fully address the relative importance of surface area of the porous media. This is important because the extent of retardation will be affected by 1) the affinity of the tracer for that porous material and 2) the surface area of

the porous media. Both quartz sand and silica beads were chosen to highlight the importance of surface area (as well as tortuosity). However, the difference in surface area and the affinity of PMCP for silica was not high enough to produce significant differences in retention times.

Among the materials tested, PMCP has the highest retardation factor on illite. This may be caused by 1) illite having the highest surface area of all porous media tested and/or 2) PMCP having the highest affinity for illite of all the column materials. These experiments do not conclude with great confidence that illite is the most adsorptive material tested; the high organic soil (C-soil) has a much lower total retardation factor but also has a much lower surface area. The relative contribution of surface area vs. affinity cannot be untangled from these data.

The relative influence of surface area and affinity is important for evaluating whether or not the tracer will be significantly retarded in a vadose zone of interest. The best way to resolve the influence of surface area and affinity is to find the Langmuir constant for that particular media and tracer. This is commonly done using a commercial BET analyzer with the tracer as the adsorbing gas (Ji et al., 2012) or using a transient diffusion experiment (Shonnard et al., 1993).

5.2.2 Water Content and Sorption

Water content is a very important consideration for vadose zone gas transport and adsorption processes and was not considered in these experiments. Several studies have shown that retardation factors of gases—particularly volatile organic chemicals (VOCs)—depend on the sorptive capacity of the porous medium, which varies considerably with water content. For example, Cabbar (2001) showed that dichloromethane (DCM), 1,1,1-trichloroethane (TCE) and carbon tetrachloride (CTC) were more retarded in wet columns than dry columns. Batterman et al (1995) showed that toluene and trichloroethylene retardation factors decrease significantly as soil humidity increases above 30%but that retardation of methane is not affected by humidity. Kim et al. (1998) show that retardation of n-alcohols and three chlorinated aromatic compounds (chlorobenzene, *o*-dichlorobenzene, and *o*-chlorophenol) increased with decreasing water content (Figure 5-1). These authors also note the increasing skewness of and considerable tailing of breakthrough curves as water content decreases.

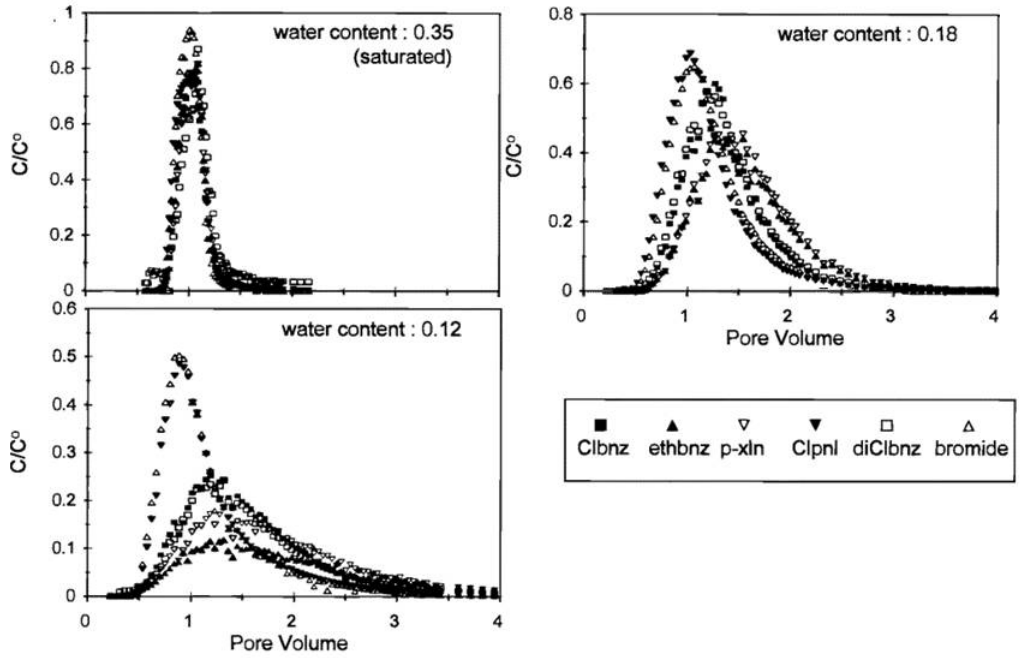

Figure 5-1: Breakthrough curves for the transport of aromatic compounds with different water contents; Cl, chloro; bnz, benzene; eth, ethyl; xln, xylene; pnl, phenol. (Kim et al., 1998)

This effect is attributed to the increase in competition between water and sorbate for sorption sites on the mineral surface. In most natural conditions, surfaces contain some adsorbed water and water vapor in pore spaces. As soil moisture or relative humidity increase, gaseous sorbents are displaced from adsorptive surfaces and thus sorption is decreased. At sufficiently high water content, surfaces are completely occupied by a monolayer of water and the Henry's law constants of the sorbing vapors becomes a very important control on sorption. Due to PFTs' low to no solubility in water, retardation is expected to be significantly decreased in the case of a monolayer of water on the porous media.

Because these experiments are run under dry conditions, retardation factors may be significantly overestimated compared to those that would be seen in real vadose zones. This is important because sorption of PFTs by hydrated vadose zone materials should be described using a multimechanistic approach, incorporating adsorption on the mineral surfaces or organic matter, adsorption at the gas-liquid interface, and dissolution into adsorbed water (Pennell et al., 1992).

5.3 IMPLICATIONS FOR CCS

This work demonstrates non-conservative behavior of PFTs in vadose zone-type material due to sorption as well as condensation to the liquid phase. Although conditions in a natural environment, such as soil moisture, may cause a decrease in PMCP sorption than that seen in these experiments, PFT flux to the NSMZ is an unreliable measure to quantify leakage rates from the injection zone. Those projects that use PFT concentrations to the NSMZ have likely underestimated leakage (e.g. Wells et al., 2007).

However, these observations do not completely invalidate the utility of PFTs, particularly in the case of historical injections. Operators and shareholders may not want to use tracers for quantifying leakage from the injection zone. Rather, the purpose of tracers may be to first detect leakage pathways from the injection zone and potential presence of injected CO_2. The primary goal of a monitoring program should be detecting whether or not leakage to the NSMZ exists and then, if detected, the leakage can be located and quantified. A monitoring program that aims to quantify leakage a priori

would be unnecessarily costly and potentially imprecise because it would not be tailored to the specific leakage (Hepple and Benson, 2005).

In this context, PFT flux to the NSMZ from historical PFT injections can still serve as a leakage indicator. Though sorption of PFT from the reservoir to the NSMZ may occur, flux of PFT to the NSMZ is an unequivocal indicator of a leakage pathway. By contrast, zero flux of tracer to the NSMZ does not necessarily indicate zero leakage pathways from the injection zone, even if the tracer is completely conservative; this assertion is a logical fallacy.

For future CCS projects, PFT retardation in the NSMZ must be considered. This study provides clear evidence that non-conservative behavior of PFTs has not been adequately tested. Because only one PFT and five porous media were considered, more analyses are needed to fully characterize PFT behavior in the NSMZ. Alternative tracers, such as SF_6, noble gases, or isotopically labeled gases should be considered good compliments to PFTs, to be used in addition to or in lieu of PFTs for future projects. Additionally, PFTs may still be useful for interwell tracing for both CCS and EOR to determine the extent of CO_2 sweep, as in Ljosland et al. (1993).

6. Conclusions

Previous studies using PFTs for leak detection and quantification in the NSMZ for CCS have relied on the assumption that PFTs exhibit conservative behavior in the near-surface. This assumption was brought into question by laboratory studies showing PFT partitioning into LNAPLs in contaminated soils (Deeds et al., 2000) and tested in the present work using packed column flow through experiments. This work shows that PFTs are retarded with respect to the conservative tracer, SF_6, on uncontaminated vadose zone materials, indicating non-conservative behavior of PFT. Non-conservative behavior is most likely due to sorption of PFT onto clays and soil organic matter or condensation to the liquid phase. Sorption onto clays appears to be the most significant factor.

Appendix: Nomenclature

Symbol	Units	Definition
v	[LT^{-1}],	Average linear flow velocity
Q	[L^3t^{-1}]	Flow rate
ϕ	[-]	porosity
A	[L^2]	Cross sectional area of column
C	[ML^{-3}]	Tracer concentration
$\alpha_L v$	[L^2 t^{-1}]	Coefficient of mechanical dispersion
L	[L]	Length of column
F	[$ML^{-2}T^{-1}$]	Flux of tracer
D_{ij}	[L^2T^{-1}]	Diffusion coefficient for gas tracer *i* into carrier gas *j*
D^*	[L^2T^{-1}]	Effective diffusion coefficient
ω	[-]	Tortuosity coefficient
D_L	[L^2T^{-1}]	Hydrodynamic dispersion coefficient
Pe	[-]	Péclet number
d	[L]	Average grain size diameter
SSA	[L^3M^{-1}]	Specific surface area
m_p	[M]	Mass of packed column
m_e	[M]	Mass of the empty column
ρ_m	[ML^{-3}]	Density of packing material *m*
V_m	[L^3]	Volume of packing material in column
V_t	[L^3]	Total volume of column
V_p	[L^3]	Pore volume of column
$\bar{t}_1$	[t]	Mean residence time (1st moment) for non-reactive tracer
$\bar{t}_2$	[t]	Mean residence time (1st moment) for reactive tracer
$K_{a,N}^i$	[-]	Partition coefficient of tracer *i* between the adsorbed phase (a) and the carrier gas (N)
R_f	[-]	Retardation factor

7. References

Albrecht, B.A., and Benson, C.H., 2001, Effect of desiccation on compacted natural clays: Journal of Geotechnical and Geoenvironmental Engineering, v. 127, no. 1, p. 67–75, doi: 10.1061/(ASCE)1090-0241(2001)127:1(67).

Artinger, R., Kienzler, B., Schüßler, W., and Kim, J., 1998, Effects of humic substances on the migration in a sandy aquifer: column experiments with Gorleben groundwater/sediment systems: Journal of Contaminant Hydrology, v. 35, no. 1-3, p. 261–275, doi: 10.1016/S0169-7722(98)00124-7.

Augier, F., 2002, On the risk of cracking in clay drying: Chemical Engineering Journal, v. 86, no. 1-2, p. 133–138, doi: 10.1016/S1385-8947(01)00279-0.

Batterman, S., Jia, C., Hatzivasilis, G., and Godwin, C., 2006, Simultaneous measurement of ventilation using tracer gas techniques and VOC concentrations in homes, garages and vehicles: Journal of Mnvironmental Monitoring, v. 8, no. 2, p. 249–56, doi: 10.1039/b514899e.

Batterman, S., Kulshrestha, A., and Cheng, H.Y., 1995, Hydrocarbon vapor transport in low moisture soils: Environmental Science & Technology, v. 29, no. 1, p. 171–80, doi: 10.1021/es00001a022.

Bear, J., 1979, Hydraulics of Groundwater: McGraw-Hill, New York.

Bégin, L., Fortin, J., and Caron, J., 2003, Evaluation of the fluoride retardation factor in unsaturated and undisturbed soil columns: Soil Science Society of America Journal, v. 67, no. 6, p. 1635–1646.

Bera, P.P., Horný, L., and Schaefer, H.F., 2004, Cyclic perfluorocarbon radicals and anions having high global warming potentials (GWPs): structures, electron affinities, and vibrational frequencies: Journal of the American Chemical Society, v. 126, no. 21, p. 6692–702, doi: 10.1021/ja0305297.

Boynton, S., and Daniel, D., 2008, Hydraulic conductivity tests on compacted clay: Journal of Geotechnical Engineering, v. 111, no. 4, p. 465–478, doi: 10.1061/(ASCE)0733-9410(1985)111:4(465).

Breus, I.P., and Mishchenko, A.A., 2006, Sorption of volatile organic contaminants by soils (a review): Eurasian Soil Science, v. 39, no. 12, p. 1271–1283, doi: 10.1134/S1064229306120015.

Buergisser, C.S., Cernik, M., Borkovec, M., and Sticher, H., 1993, Determination of nonlinear adsorption isotherms from column experiments: an alternative to batch studies: Environmental Science & Technology, v. 27, no. 5, p. 943–948, doi: 10.1021/es00042a018.

Busenberg, E., and Plummer, L.N., 2000, Dating young groundwater with sulfur hexafluoride: natural and anthropogenic sources of sulfur hexafluoride: Water Resources Research, v. 36, no. 10, p. 3011–3030, doi: 10.1029/2000WR900151.

Cabbar, H.C., and Bostanci, A., 2001, Moisture effect on the transport of organic vapors in sand: Journal of Hazardous Materials, v. 82, no. 3, p. 313–322, doi: 10.1016/S0304-3894(01)00177-7.

Caldeira, K., and Wickett, M.E., 2003, Oceanography: anthropogenic carbon and ocean pH.: Nature, v. 425, no. 6956, p. 365, doi: 10.1038/425365a.

Cannavo, P., Lafolie, F., Nicolardot, B., and Renault, P., 2006, Modeling seasonal variations in carbon dioxide and nitrous oxide in the vadose zone: Vadose Zone Journal, v. 5, no. 3, p. 990–1004, doi: 10.2136/vzj2005.0124.

Chang, S., Lincoff, H., Zimmermann, N.J., and Fuchs, W., 1989, Giant retinal tears-surgical techniques and results using perfluorocarbon liquids: Archives of Ophtamology, v. 107, no. 5, p. 761–766.

Communar, G., Keren, R., and Li, F., 2004, Deriving boron adsorption isotherms from soil column displacement experiments: Soil Science Society of America Journal, v. 68, no. 2, p. 481–488, doi: 10.2136/sssaj2004.4810.

Cooke, K.M., Simmonds, P.G., Nickless, G., and Makepeace, A.P.W., 2001, Use of capillary gas chromatography with negative ion-chemical ionization mass spectrometry for the determination of perfluorocarbon tracers in the atmosphere: Analytical Chemistry, v. 73, no. 17, p. 4295–4300, doi: 10.1021/ac001253d.

Cortis, A., Oldenburg, C.M., and Benson, S.M., 2008, The role of optimality in characterizing CO_2 seepage from geologic carbon sequestration sites: International Journal of Greenhouse Gas Control, v. 2, no. 4, p. 640–652, doi: 10.1016/j.ijggc.2008.04.008.

Darcy, H., 1856, Les fontaines publiques de la ville de Dijon (V. Dalmont, Ed.): Dalmont.

Darnault, C.J.G., Steenhuis, T.S., Garnier, P., Kim, Y.J., Jenkins, M.B., Ghiorse, W.C., Baveye, P.C., and Parlange, J.Y., 2004, Preferential flow and transport of Cryptosporidium parvum oocysts through the vadose zone: Experiments and modeling: Vadose Zone Journal, v. 3, no. 1, p. 262–270.

Day, R.W., 1997, Discussion of "Hydraulic Conductivity of Desiccated Geosynthetic Clay Liners" by Tom Boardman and David E. Daniel: Journal of Geotechnical and Geoenvironmental Engineering, v. 123, no. 5, p. 484–486, doi: 10.1061/(ASCE)1090-0241(1997)123:5(484.2).

Deeds, N.E., McKinney, D.C., and Pope, G.A., 2000, Laboratory characterizatio nof non-aqueous phase liquid/tracer interaction in support of a vadose zone partitioning interwell tracer test: Journal of Contaminatn Hydrogeology, v. 41, p. 193–204.

Deeds, D.A., Vollmer, M.K., Kulongoski, J.T., Miller, B.R., Mühle, J., Harth, C.M., Izbicki, J.A., Hilton, D.R., and Weiss, R.F., 2008, Evidence for crustal degassing of CF4 and SF_6 in Mojave Desert groundwaters: Geochimica et Cosmochimica Acta, v. 72, no. 4, p. 999–1013, doi: 10.1016/j.gca.2007.11.027.

Demokritou, P., Yang, C., Chen, Q., and D. Spengler, J., 2002, An experimental method for contaminant dispersal characterization in large industrial buildings for indoor air quality (IAQ) applications: Building and Environment, v. 37, no. 3, p. 305–312, doi: 10.1016/S0360-1323(01)00018-X.

Dietz, R.N., 1986, Perfluorocarbon Tracer Technology (S. Sandroni, Ed.): Regional and Long-range Transport of Air Pollution: Lectures,, p. 215–247.

DOE/NETL, 2012, Monitoring, Verification, and Accounting (MVA) of CO_2 Stored in Deep Geologic Formations - 2012 Update, DOE/NETL/1568.

Doney, S.C., Fabry, V.J., Feely, R.A., and Kleypas, J.A., 2009, Ocean acidification: the other CO_2 problem: Annual Review of Marine Science, v. 1, no. 1, p. 169–192, doi: 10.1146/annurev.marine.010908.163834.

Dugstad, Ø., Bjørnstad, T., and Hundere, I.A., 1993, Measurements of gas tracer retention under simulated reservoir conditions: Journal of Petroleum Science and Engineering, v. 10, no. 1, p. 17–25, doi: 10.1016/0920-4105(93)90047-I.

EIA, 2011, Annual Energy Outlook 2011: U.S. Energy Information Administration, DOE/EIA-0383(2011).

Fetter, C.W., 1994, Applied Hydrogeology: Prentice Hall, Upper Saddle River.

Fetter, C.W., 1999, Contaminant Hydrology: Waveland Press, Inc., Long Grove, IL.

Freifeld, B., Trautz, R., Kharaka, Y., Phelps, T., Myer, L., Hovorka, S., and Collins, D., 2005, The U-tube: A novel system for acquiring borehole fluid samples from a deep geologic CO_2 sequestration experiment : Journal of Geophysical Research, v. 110.

Fuller, E.N., Schettle, P.D., and Giddings, J.C., 1966, A new method for prediction of binary gas-phase diffusion coefficients: Industrial and Engineering Chemistry, v. 58, no. 5, p. 19–27, doi: 10.1021/ie50677a007.

Gaines, R. V., Skinner, H.C.W., Foord, E.E., Mason, B., and Rosenzweig, A., 1997, Dana's new mineralogy: Wiley, New York.

Gamlin, J.D., Clark, J.F., Woodside, G., and Herndon, R., 2001, Large-scale tracing of ground water with sulfur hexafluoride: Journal of Environmental Engineering, v. 127, no. 2, p. 171–174, doi: 10.1061/(ASCE)0733-9372(2001)127:2(171).

Ghafurian, R., Dietz, R.N., Rodenbaugh, T., Dominguez, J., and Tai, N., 1999, Leak location in fluid filled cables using the PFT method: IEEE Transactions on Power Delivery, v. 14, no. 1, p. 18–22, doi: 10.1109/61.736673.

Gooddy, D.C., Darling, W.G., Abesser, C., and Lapworth, D.J., 2006, Using chlorofluorocarbons (CFCs) and sulphur hexafluoride (SF_6) to characterise groundwater movement and residence time in a lowland Chalk catchment: Journal of Hydrology, v. 330, no. 1-2, p. 44–52, doi: 10.1016/j.jhydrol.2006.04.011.

Grolimund, D., Borkovec, M., Federer, P., and Sticher, H., 1995, Measurement of sorption isotherms with flow-through reactors: Environmental Science & Technology, v. 29, no. 9, p. 2317–21, doi: 10.1021/es00009a025.

Gschwend, P.M., and Wu, S., 1985, On the constancy of sediment-water partition coefficients of hydrophobic organic pollutants: Environmental Science & Technology, v. 19, no. 1, p. 90–96, doi: 10.1021/es00131a011.

Heiser, J., Sullivan, T., and Serrato, M., 2005, Long-term verification of cover systems using perfluorocarbon tracers: Journal of Environmental Engineering, v. 131, no. 6, p. 952–960, doi: 10.1061/(ASCE)0733-9372(2005)131:6(952).

Hepple, R.P., and Benson, S.M., 2005, Geologic storage of carbon dioxide as a climate change mitigation strategy: performance requirements and the implications of surface seepage: Environmental Geology, v. 47, no. 4, p. 576–585, doi: 10.1007/s00254-004-1181-2.

Hovorka, S.D., Meckel, T.A., Trevino, R.H., Lu, J., Nicot, J.-P., Choi, J.-W., Freeman, D., Cook, P., Daley, T.M., Ajo-Franklin, J.B., Freifeild, B.M., Doughty, C., Carrigan, C.R., Brecque, D. La, et al., 2011, Monitoring a large volume CO_2 injection: Year two results from SECARB project at Denbury's Cranfield, Mississippi, USA: Energy Procedia, v. 4, p. 3478–3485, doi: 10.1016/j.egypro.2011.02.274.

Hsu, J.T., and Chen, T.-L., 1987, Theoretical analysis of the asymmetry in chromatographic peaks: Journal of Chromatography A, v. 404, p. 1–9, doi: 10.1016/S0021-9673(01)86831-X.

IEA, 2009, Technology Roadmap: Carbon capture and storage: International Energy Agency, Paris.

IPCC, 2007, Climate Change 2007: Synthesis Report. Contribution of Working Groups I, II and III to the Fourth Assessment Report of the Intergovernmental Panel on Climate Change [Core Writing Team, Pachauri, R.K and Reisinger, A. (eds)]: IPCC, Geneva, Switzerland, 104 pp.

IPCC, 2005, IPCC special report on carbon dioxide capture and storage. Prepared by working group III of the Intergovernmental Panel on Climate Change, *in* Metz, B., Davidson, O., De Coninck, H.C., Loos, M., and Meyer, L.A. eds., IPCC Special Report on Carbon Dioxide Capture and Storage, Cambridge University Press, p. 442.

Jackson, D.R., Garrett, B.C., and Bishop, T.A., 1984, Comparison of batch and column methods for assessing leachability of hazardous waste: Environmental Science & Technology, v. 18, no. 9, p. 668–673, doi: 10.1021/es00127a007.

Ji, L., Zhang, T., Milliken, K.L., Qu, J., and Zhang, X., 2012, Experimental investigation of main controls to methane adsorption in clay-rich rocks: Applied Geochemistry, v. 27, no. 12, p. 2533–2545, doi: 10.1016/j.apgeochem.2012.08.027.

Jin, M., Delshad, M., Dwarakanath, V., McKinney, D.C., Pope, G.A., Sepehrnoori, K., Tilburg, C.E., and Jackson, R.E., 1995, Partitioning tracer test for detection, estimation, and remediation performance assessment of subsurface nonaqueous phase liquids: Water Resources Research, v. 31, no. 5, p. 1201, doi: 10.1029/95WR00174.

Jin, Y., Yates, M.V., Thompson, S.S., and Jury, W.A., 1997, Sorption of viruses during flow through saturated sand columns: Environmental Science & Technology, v. 31, no. 2, p. 548–555, doi: 10.1021/es9604323.

Joughin, I., Alley, R.B., and Holland, D.M., 2012, Ice-sheet response to oceanic forcing.: Science, v. 338, no. 6111, p. 1172–6, doi: 10.1126/science.1226481.

Keller, J.M., and Brusseau, M.L., 2003, In-situ characterization of soil−water content using gas-phase partitioning tracer tests: Field-scale evaluation: Environmental Science & Technology, v. 37, no. 14, p. 3141–3144, doi: 10.1021/es0340329.

Kim, H., Annable, M.D., and Rao, P.S.C., 1998, Influence of air−water interfacial adsorption and gas-phase partitioning on the transport of organic chemicals in unsaturated porous media: Environmental Science & Technology, v. 32, no. 9, p. 1253–1259, doi: 10.1021/es970868y.

Klein, C., and Dutrow, B., 2008, Manual of Mineral Science: John Wiley & Sons, Inc., Hoboken.

Klein, M., Müller, M., Dust, M., Görlitz, G., Gottesbüren, B., Hassink, J., Kloskowski, R., Kubiak, R., Resseler, H., Schäfer, H., Stein, B., and Vereecken, H., 1997, Validation of the pesticide leaching model PELMO using lysimeter studies performed for registration: Chemosphere, v. 35, no. 11, p. 2563–2587, doi: 10.1016/S0045-6535(97)00325-1.

Klusman, R.W., 2011, Comparison of surface and near-surface geochemical methods for detection of gas microseepage from carbon dioxide sequestration: International Journal of Greenhouse Gas Control, v. 5, no. 6, p. 1369–1392, doi: 10.1016/j.ijggc.2011.07.014.

Koestel, J.K., Moeys, J., and Jarvis, N.J., 2012, Meta-analysis of the effects of soil properties, site factors and experimental conditions on solute transport: Hydrology and Earth System Sciences, v. 16, no. 6, p. 1647–1665, doi: 10.5194/hess-16-1647-2012.

Kool, J., Parker, J., and Zelazny, L., 1989, On the estimation of cation-exchange parameters from column displacement experiments: Soil Science Society of America Journal, v. 53, no. 5, p. 134701355.

Langston, E.P., and Shirer, J.A., 1985, Performance of Jay/LEC fields unit under mature waterflood and early tertiary operations: Journal of Petroleum Technology, v. 37, no. 2, p. 261–268.

Ledwell, J.R., Watson, A.J., and Law, C.S., 1993, Evidence for slow mixing across the pycnocline from an open-ocean tracer-release experiment: Nature, v. 364, no. 6439, p. 701–703, doi: 10.1038/364701a0.

Leij, F.J., Toride, N., Field, M.S., and Sciortino, A., 2012, Solute transport in dual-permeability porous media: Water Resources Research, v. 48, no. 4, p. n/a–n/a, doi: 10.1029/2011WR011502.

Lenhoff, A.M., 1987, Significance and estimation of chromatographic parameters: Journal of Chromatography A, v. 384, p. 285–299, doi: 10.1016/S0021-9673(01)94678-3.

Levenspiel, O., 1972, Chemical reaction engineering: Wiley, New York.

Levin, I., and Hesshaimer, V., 1996, Refining of atmospheric transport model entries by the globally observed passive tracer distributions of 85 krypton and sulfur hexafluoride (SF_6): Journal of Geophysical Research, v. 101, no. D11, p. 16745, doi: 10.1029/96JD01058.

Lewicki, J.L., 2005, An improved strategy to detect CO_2 leakage for verification of geologic carbon sequestration: Geophysical Research Letters, v. 32, no. 19, p. L19403, doi: 10.1029/2005GL024281.

Lewis, J., and Sjöstrom, J., 2010, Optimizing the experimental design of soil columns in saturated and unsaturated transport experiments: Journal of Contaminant Hydrology, v. 115, no. 1-4, p. 1–13, doi: 10.1016/j.jconhyd.2010.04.001.

Lion, L.W., Stauffef, T.B., and MacIntyre, W.G., 1990, Sorption of hydrophobic compounds on aquifer materials: analysis methods and the effect of organic carbon: Journal of Contaminant Hydrology, v. 5, no. 3, p. 215–234, doi: 10.1016/0169-7722(90)90038-I.

Ljosland, E., Bjornstad, T., Dugstad, O., and Hundere, I., 1993, Perfluorocarbon tracer studies at the Gullfaks field in the North Sea: Journal of Petroleum Science and Engineering, v. 10, no. 1, p. 27–38, doi: 10.1016/0920-4105(93)90048-J.

Lovelock, J.E., and Ferber, G.J., 1982, Exotic tracers for atmospheric studies: Atmospheric Environment (1967), v. 16, no. 6, p. 1467–1471, doi: 10.1016/0004-6981(82)90069-5.

Luo, Y., and Zhou, X., 2006, Soil Respiration and the Environment: Elsevier, Amsterdam.

MacIntyre, W.G., and Stauffer, T.B., 1988, Liquid chromatography applications to determination of sorption on aquifer materials: Chemosphere, v. 17, no. 11, p. 2161–2173, doi: 10.1016/0045-6535(88)90164-6.

Maraqa, M.A., Zhao, X., Wallace, R.B., and Voice, T.C., 1998, Retardation coefficients of nonionic organic compounds determined by batch and column techniques: Soil Science Society of America Journal, v. 62, no. 1, p. 142, doi: 10.2136/sssaj1998.03615995006200010019x.

Mariner, P.E., Jin, M., Studer, J.E., and Pope, G.A., 1999, The first vadose zone partitioning interwell tracer test for nonaqueous phase liquid and water residual: Environmental Science & Technology, v. 33, no. 16, p. 2825–2828, doi: 10.1021/es9901720.

Maxfield, B.T., Ginosar, D.M., McMurtrey, R.D., Rollins, H.W., and Shook, G.M., 2005, The effect of moisture content on retention of fluorocarbon tracers on sand: Geothermics, v. 34, no. 1, p. 47–60, doi: 10.1016/j.geothermics.2004.06.003.

McCallum, S.D., Riestenberg, D.E., Cole, D.R., Freifeld, B., Trautz, R.C., Hovorka, S.D., and Phelps, T., 2005, Monitoring geologically sequestered CO_2 during the Frio Brine pulot test using perfluorocarbon tracers, *in* Fouth Annual Conference on Carbon Capture and Sequestration DOE/NETL,.

Mibus, J., Sachs, S., Pfingsten, W., Nebelung, C., and Bernhard, G., 2007, Migration of uranium(IV)/(VI) in the presence of humic acids in quartz sand: a laboratory column study: Journal of Contaminant Hydrology, v. 89, no. 3-4, p. 199–217, doi: 10.1016/j.jconhyd.2006.08.005.

MIT, 2007, The future of coal options for a carbon-constrained world: Massachusetts Institue of Technology, Boston.

Nelson, N.T., Brusseau, M.L., Carlson, T.D., Costanza, M.S., Young, M.H., Johnson, G.R., and Wierenga, P.J., 1999, A gas-phase partitioning tracer method for the in situ measurement of soil-water content: Water Resources Research, v. 35, no. 12, p. 3699–3707, doi: 10.1029/1999WR900250.

NETL, 2012, The North American Carbon Storage Atlas: National Energy Technology Laboratory.

Neuman, S.P., 1990, Universal scaling of hydraulic conductivities and dispersivities in geologic media: Water Resources Research, v. 26, no. 8, p. 1749–1758, doi: 10.1029/90WR00596.

Olschewski, A., Fischer, U., Hofer, M., and Schulin, R., 1995, Sulfur hexafluoride as a gas tracer in soil venting operations: Environmental Science & Technology, v. 29, no. 1, p. 264–6, doi: 10.1021/es00001a034.

Omoregie, Z.S., Vasicek, S.L., Jackson, G.R., and Martinson, L.A., 1988, Monitoring the Mitsue hydrocarbon miscible flood—program design, implementation and preliminary results: Journal of Canadian Petroleum Technology, v. 27, no. 6, p. 51–62.

Orr, J.C., Fabry, V.J., Aumont, O., Bopp, L., Doney, S.C., Feely, R.A., Gnanadesikan, A., Gruber, N., Ishida, A., Joos, F., Key, R.M., Lindsay, K., Maier-Reimer, E., Matear, R., et al., 2005, Anthropogenic ocean acidification over the twenty-first century and its impact on calcifying organisms: Nature, v. 437, no. 7059, p. 681–6, doi: 10.1038/nature04095.

Pennell, K.D., Rhue, R.D., Rao, P.S.C., and Johnston, C.T., 1992, Vapor-phase sorption of p-xylene and water on soils and clay minerals: Environmental Science & Technology, v. 26, no. 4, p. 756–763, doi: 10.1021/es00028a014.

Perkins, T.K., and Johnston, O.C., 1963, A review of diffusion and dispersion in porous media: Society of Petroleum Engineers Journal, v. 3, no. 1, p. 70–84.

Piatt, J.J., Backhus, D.A., Capel, P.D., and Eisenreich, S.J., 1996, Temperature-dependent sorption of naphthalene, phenanthrene, and pyrene to low organic carbon aquifer sediments: Environmental Science & Technology, v. 30, no. 3, p. 751–760, doi: 10.1021/es9406288.

Plummer, L.N., Busenberg, E., Böhlke, J.K., Nelms, D.L., Michel, R.L., and Schlosser, P., 2001, Groundwater residence times in Shenandoah National Park, Blue Ridge

Mountains, Virginia, USA: a multi-tracer approach: Chemical Geology, v. 179, no. 1-4, p. 93–111, doi: 10.1016/S0009-2541(01)00317-5.

Regulation(EC) No 842/2006 of the European Parliament and of the Council of 17 May 2006 on certain fluorinated greenhouse gases, 2006, Official Journal of the European Union, v. 161, no. 2.

Reimus, P.W., Watson, T., Vermeul, V., Newell, D., and Williams, M., 2011, Laboratory testing and modeling to evaluate perflurorocarbon compounds as tracers in geothermal systems: Proceedings: Thirty-Sixth Workshop on Geothermal Reservoir Engineering, p. 1–9.

Rigby, M., Mühle, J., Miller, B.R., Prinn, R.G., Krummel, P.B., Steele, L.P., Fraser, P.J., Salameh, P.K., Harth, C.M., Weiss, R.F., Greally, B.R., O'Doherty, S., Simmonds, P.G., Vollmer, M.K., et al., 2010, History of atmospheric SF_6 from 1973 to 2008: Atmospheric Chemistry and Physics, v. 10, p. 10305–10320, doi: 10.5194/acp-10-10305-2010.

Santella, N., Ho, D.T., Schlosser, P., and Stute, M., 2003, Distribution of atmospheric SF_6 near a large urban area as recorded in the vadose zone: Environmental Science & Technology, v. 37, no. 6, p. 1069–1074, doi: 10.1021/es0156993.

Sardin, M., Schweich, D., Leij, F.J., and Th. van Genuchten, M., 1991, Modeling the nonequilibrium transport of linearly interacting solutes in porous media: A review: Water Resources Research, v. 27, no. 9, p. 2287–2307, doi: 10.1029/91WR01034.

Schloemer, S., Furche, M., Dumke, I., Poggenburg, J., Bahr, A., Seeger, C., Vidal, A., and Faber, E., 2013, A review of continuous soil gas monitoring related to CCS–Technical advances and lessons learned: Applied Geochemistry, v. 30, no. null, p. 148–160, doi: 10.1016/j.apgeochem.2012.08.002.

Schumacher, B.A., 2002, Methods for the Determination of Total Organic Carbon (TOC) in Soils and Sediments: EPA, NCEA-C-1282 EMASC-001.

Schütze, C., Sauer, U., Beyer, K., Lamert, H., Bräuer, K., Strauch, G., Flechsig, C., Kämpf, H., and Dietrich, P., 2012, Natural analogues: a potential approach for developing reliable monitoring methods to understand subsurface CO_2 migration processes: Environmental Earth Sciences, v. 67, no. 2, p. 411–423, doi: 10.1007/s12665-012-1701-4.

Schweich, D., Sardin, M., and Gaudet, J.-P., 1982, Measurement of a cation exchange isotherm from elution curves obtained in a soil column: Preliminary results: Soil Science Society of America Journal, v. 47, no. 1, p. 32–37.

Senum, G.I., D'Ottavio, T.W., Loss, W.M., Goodrich, R.W., Spandau, D.J., and Dietz, R.N., 1997, HPFF cable leak location using perfluorocarbon tracers: Final report: Electric Power Research Institute, TR-109086 7905-01.

Senum, G.I., Fajer, R., DeRose, W.E., Harris Jr., B.R., and Ottaviani, W.L., 1992, Petroleum reservoir characterization by perfluorocarbon tracers: Enhanced oil recovery symposium, p. 337–345.

Shepherd, A., Ivins, E.R., A, G., Barletta, V.R., Bentley, M.J., Bettadpur, S., Briggs, K.H., Bromwich, D.H., Forsberg, R., Galin, N., Horwath, M., Jacobs, S., Joughin, I., King, M.A., et al., 2012, A reconciled estimate of ice-sheet mass balance: Science, v. 338, no. 6111, p. 1183–9, doi: 10.1126/science.1228102.

Shonnard, D.R., Bell, R.L., and Jackman, A.P., 1993, Effects of nonlinear sorption on the diffusion of benzene and dichloromethane from two air-dry soils: Environmental Science & Technology, v. 27, no. 3, p. 457–466, doi: 10.1021/es00040a002.

Shook, G.M., 2005, A systematic method for tracer test analysis: An example using Beowawe tracer data: Proceedings, Thirtieth Workshop on Geothermal Reservoir Engineering, Stanford University, Stanford, California, SGP-TR-176.

Šimůnek, J., Jarvis, N.J., Van Genuchten, M.T., and Gärdenäs, A., 2003, Review and comparison of models for describing non-equilibrium and preferential flow and transport in the vadose zone: Journal of Hydrology, v. 272, no. 1-4, p. 14–35, doi: 10.1016/S0022-1694(02)00252-4.

De Smedt, F., and Wierenga, P.J., 1979, A generalized solution for solute flow in soils with mobile and immobile water: Water Resources Research, v. 15, no. 5, p. 1137–1141, doi: 10.1029/WR015i005p01137.

Sonnerup, R.E., Mecking, S., and Bullister, J.L., 2013, Transit time distributions and oxygen utilization rates in the Northeast Pacific Ocean from chlorofluorocarbons and sulfur hexafluoride: Deep Sea Research Part I: Oceanographic Research Papers, v. 72, p. 61–71, doi: 10.1016/j.dsr.2012.10.013.

Spada, G., Bamber, J.L., and Hurkmans, R.T.W.L., 2013, The gravitationally consistent sea-level fingerprint of future terrestrial ice loss: Geophysical Research Letters, v. 40, no. 3, p. 482–486, doi: 10.1029/2012GL053000.

Stalker, L., Boreham, C., Underschultz, J., Freifeld, B., Perkins, E., Schacht, U., and Sharma, S., 2009, Geochemical monitoring at the CO2CRC Otway Project: Tracer injection and reservoir fluid acquisition: Energy Procedia, v. 1, no. 1, p. 2119–2125, doi: 10.1016/j.egypro.2009.01.276.

Stoessell, R.K., 1999, Predicted retardations of concentration fronts using a mass-balance approach: Ground water, v. 37, no. 5, p. 701–706, doi: 10.1111/j.1745-6584.1999.tb01162.x.

Sullivan, T.M., Heiser, J., Gard, A., and Senum, G., 1996, Monitoring subsurface barrier integrity using perfluorocarbon tracers: Journal of Environmental Engineering, v. 124, no. 6, p. 490–497, doi: 10.1061/(ASCE)0733-9372(1998)124:6(490) .

Tang, J.S., and Harker, B., 1991, Interwell tracer test to determine residual oil saturation in a gas-saturated reservoir part II: Field applications: Journal of Canadian Petroleum Technology, v. 30, no. 4, p. 34–44, doi: 10.2118/91-04-01.

Thomas, R., Rignot, E., Casassa, G., Kanagaratnam, P., Acuña, C., Akins, T., Brecher, H., Frederick, E., Gogineni, P., Krabill, W., Manizade, S., Ramamoorthy, H., Rivera, A., Russell, R., et al., 2004, Accelerated sea-level rise from West Antarctica: Science, v. 306, no. 5694, p. 255–258, doi: 10.1126/science.1099650.

Tick, G.R., McColl, C.M., Yolcubal, I., and Brusseau, M.L., 2007, Gas-phase diffusive tracer test for the in-situ measurement of tortuosity in the vadose zone: Water, Air, and Soil Pollution, v. 184, no. 1-4, p. 355–362, doi: 10.1007/s11270-007-9403-3.

USDOD, 2012, Emerging Chemical and Material Risks: DENIX: DoD Environment, Safety and Occupational Health Network and Information Exchange.

USEPA, 2013, Geologic Sequestration of Carbon Dioxide: Underground Injection Control (UIC) Program Class VI Well Testing and Monitoring Guidance: Washington, D.C.

USEPA, 2010, Mandatory Reporting of Greenhouse Gases:Injection and Geologic Sequestration of Carbon Dioxide; Final Rule: Washington, D.C.

USEPA, 2011, Mandatory Reporting of Greenhouse Gases: Additional Sources of Fluorinated GHGs; Final Rule : Washington, D.C.

Varani, J., Hirschl, R.B., Dame, M., and Johnson, K., 1996, Perfluorocarbon protects lung epithelial cells from neutrophil-mediated injury in an in vitro model of liquid ventilation therapy: Shock, v. 6, no. 5, p. 339–344, doi: 10.1097/00024382-199611000-00007.

Watson, T.B., and Sullivan, T., 2012, Feasibility of a perfluorocarbon tracer based network to support monitoring, verification, and accounting of sequestered CO_2: Environmental Science & Technology, v. 46, no. 3, p. 1692–1699, doi: 10.1021/es2034284.

Watson, T.B., Wilke, R., Dietz, R.N., Heiser, J., and Kalb, P., 2007, The atmospheric background of perfluorocarbon compounds used as tracers: Environmental Science & Technology, v. 41, no. 20, p. 6909–6913, doi: 10.1021/es070940k.

Wells, A., Diehl, J., Bromhal, G., Strazisar, B., Wilson, T., and White, C., 2007, The use of tracers to assess leakage from the sequestration of CO2 in a depleted oil reservoir, New Mexico, USA: Applied Geochemistry, v. 22, no. 5, p. 996–1016, doi: 10.1016/j.apgeochem.2007.01.002.

Whitley, G.A.J., 1997, An investigation of partitioning tracers for characterization of nonaqueous phase liquids in vadose zones. Diss. The University of Texas at Austin. Austin, Texas.

Whitley, G.A.J., McKinney, D.C., Pope, G.A., Rouse, B.A., and Deeds, N.E., 1999, Contaminated vadose zone characterization using partitioning gas tracers: Journal of Environmental Engineering, v. 125, p. 574–582, doi: 10.1061/(ASCE)0733-9372.

Wilson, R.D., and Mackay, D.M., 1996, SF_6 as a conservative tracer in saturated media with high intragranular porosity or high organic carbon content: Ground Water, v. 34, no. 2, p. 241–249, doi: 10.1111/j.1745-6584.1996.tb01884.x.